УДК 544.42/43

Многотемпературная модель SPS реактора синтеза и уплотнения нитрида циркония

А.А. Марков

Институт проблем механики им. А.Ю. Ишлинского РАН Р.Ф. 119526, Москва, пр-т Вернадского, д. 101, корп. 1.

markov.ipm@yandex.ru

Аннотация

Модель включает температуру твердой фазы смеси Zr и ZrN, температуру газовой фазы N2, температуру корпуса реактора из пористого графита, температуру низкоомного слоя вольфрамового сплава к электродам которого приложена разность потенциалов. Предложена модель реактора искрового спекания SPS, который содержит канал для подачи газа Исследованы режимы работы реактора с многостадийным потоком азота на входе в реактор, включающие предел упругости с переходом к термопластичности для пористой смеси твердых частиц с газовой фазой, Результаты удовлетворительно согласуются с экспериментальными данными.

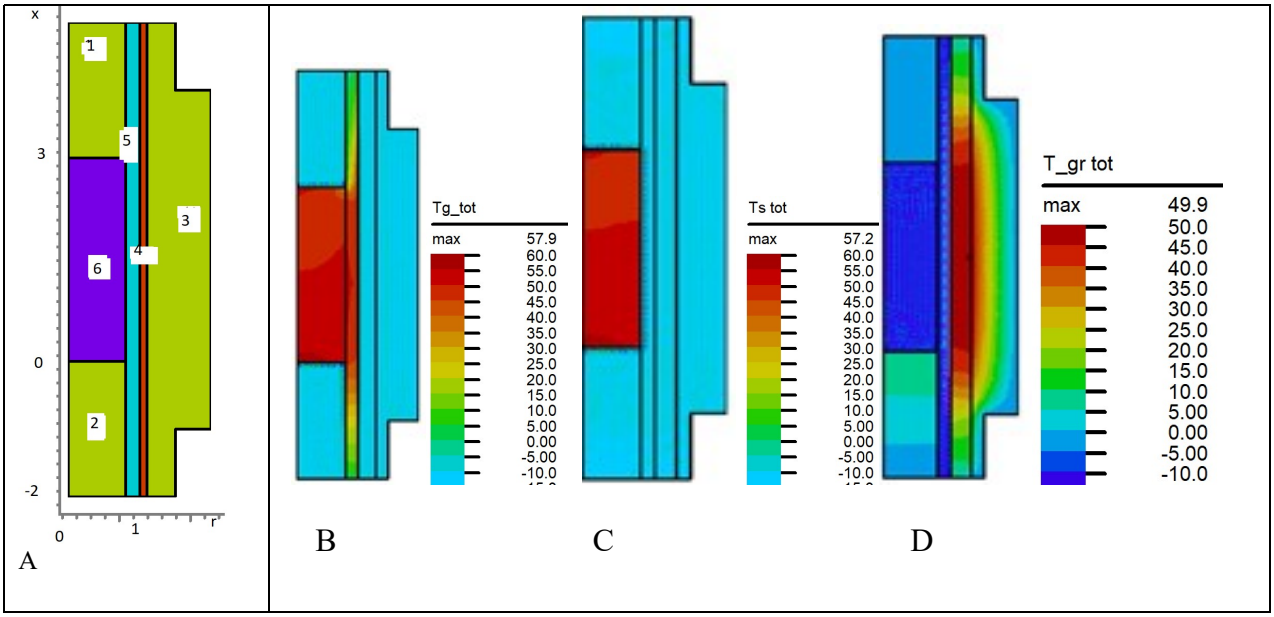

Фиг.. 1. Схема трехзонного осесимметричного реактора (Фиг. 1A). Показана область моделирования, состоящая из зон 1,…,6. Зона 1: $-2 < x < 0, 0 < r < R_1$. Зона 2: $3 < x < 5, 0 < r < R_1$. Зона 3: $-1 < x < 4, 1+\delta < r < R_2$ -графитовый корпус реактора. Зона 4: $-2 < x < 5, 1 < r < 1+\delta$ - вольфрамовый слой. Зона 5: $0 < x < 3, R_1 < r < 1$ - канал подачи N_2. Зона 6: $0 < x < 3, 0 < r < R_1$ -пористая область смеси реагентов и продуктов синтеза. На Фиг. 1B и Фиг. 1C иллюстрируется распределение температуры газа и твердой фазы в зоне 6 в момент времени $t = 0.88$. На Фиг. 1D представлено распределение температуры графитового корпуса в зонах 1,2, 3 в момент времени $t = 0.88$.

The first page (with annotation) only for English language papers

UDC 544.42/43

Multitemperature model of a SPS reactor for the synthesis and densification of zirconium nitride

A A Markov

Ishlinsky Institute for Problems in Mechanics RAS. Vernadskii ave. 101, b1, 119526,Moscow, Russia

markov.ipm@yandex.ru

Abstract

The model includes the temperature of the solid phase of the mixture of Zr, ZrN, the temperature of the gas phase N2, the temperature of the reactor vessel made of porous graphite and the temperature of the low-resistance layer of tungsten alloy to the electrodes of which a potential difference is applied. A model of an SPS spark sintering reactor with a gas supply channel is proposed. The operating modes of a reactor with a multistage nitrogen flux at the reactor inlet, including the elastic limit with a transition from thermoelasticity model to thermoplasticity one for a porous mixture of solid particles with a gas phase, are investigated. The results are in satisfactory agreement with experimental data.

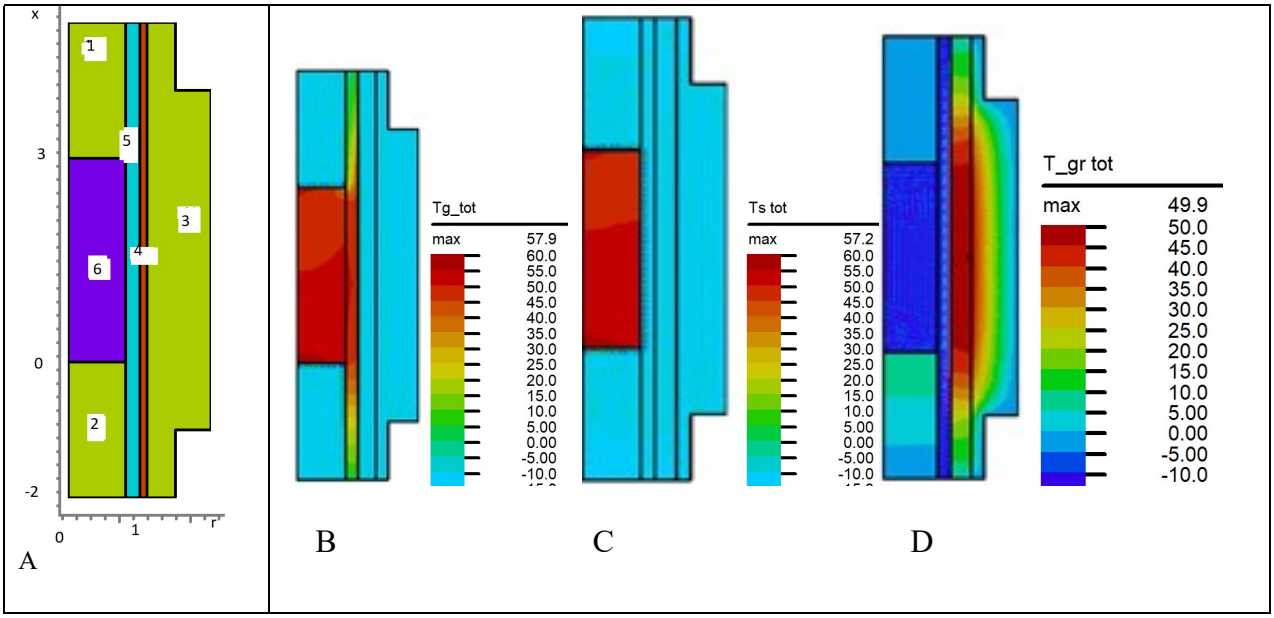

Fig .. 1. Scheme of a three-zone axisymmetric reactor (Fig. 1A). The modeling area is shown, consisting of zones 1,…, 6. Zone 1: $-2 < x < 0, 0 < r < R_1$. Zone 2: $3 < x < 5, 0 < r < R_1$. Zone 3: $-1 < x < 4, 1+\delta < r < R_2$ - graphite reactor vessel. Zone 4: $-2 < x < 5, 1 < r < 1+\delta$ - tungsten layer. Zone 5: $0 < x < 3, R_1 < r < 1$ - feed channel of N_2. Zone 6: $0 < x < 3, 0 < r < R_1$ - porous area of a mixture of reagents and synthesis products. Fig. 1B and Fig. 1C illustrates the temperature distribution of the gas and the solid phase in zone 6 at time instance $t = 0.88$. Fig. 1D shows the temperature distribution of a graphite body in zones 1, 2, 3 at time instance $t = 0.88$.

Key words: variable porosity, synthesis of zirconium nitride, SPS reactor with gas supply, multitemperature model.

1. Introduction

Zirconium nitride ZrN has attracted more and more attention in the last decade due to its combination of excellent thermal, mechanical and electrical properties, high melting point, hardness and high strength characteristics. Ceramics based on zirconium nitride are used in electrical engineering, atomic materials science and manufacturing. Ceramics ZrC and ZrN are of interest for the use the materials at extremely high temperatures. Zirconium carbide ZrC and nitride ZrN exhibit desirable characteristics such as high thermal conductivity and electrical conductivity. The data presented in the literature often suffer from scatter due to differences in processing methods and the complexity of determining stoichiometry, which significantly affects the thermophysical properties [1]. However, the methods of processing these materials can change the content of impurities such as oxygen in ZrC and oxygen and carbon in ZrN. Also, zirconium nitride is used as protective wear-resistant coatings of parts in contact with aggressive media, is a substitute for uranium nitride to optimize the parameters of the nitride fuel fabrication process, which is considered for use in space power reactors [2] and advanced emergency-resistant fuels for reactors [3,4]. Zirconium has a remarkable ability to burn in atmospheric oxygen (autoignition temperature - 250 ° C) with little or no smoke and at a high rate.This develops the highest temperature for metallic fuels (4650 ° C). Experiments were carried out on using the combustion of zirconium as a light source for pumping a laser. Zirconium and hafnium nitride are refractory (> 2500 ° C) and are close in hardness to superhard materials (24 GPa) [5,6]. These materials, having high thermal and electrical conductivity [1], are applied in microelectronics.

To obtain ZrC and ZrN, the method of self-propagating high-temperature synthesis (SHS) [7-9] and the method of chemical vapor deposition [6, 10] were used. The method for producing zirconium nitride based on SHS by burning a mixture consisting of zirconium oxide and an energy component in the presence of a nitriding agent is carried out. In the process, the intermediate products are quenched by interrupting the combustion process in 20-90 seconds after initiation, and an activating additive of oxides nanopowder is additionally incorporated into the exothermic mixture. The synthesis of carbide and nitride materials usually involves a direct reaction with a metal, metal hydride, or metal oxide, with the metal oxide being the main precursor in spent fuel reprocessing [1].

The traditional approach to obtaining materials based on fine ZrN powders [6] separates the stages of synthesis and sintering. The resulting cakes are mechanically ground in ball mills and re-nitrided. The process is repeated until the nitride yield reaches 95-98%. One of known method of obtaining zirconium nitride is a direct nitriding of zirconium powder. Zirconium powder is subjected to heat treatment at a temperature of 1200-1600 ° C in a nitrogen environment. The disadvantages of this method are high synthesis temperatures, complex instrumentation. An expensive pure nitrogen gas have to be used. There is a known method in which hydrogenated zirconium powder forms nitride at high temperatures, about 1300-1400 ° C, duiring 5 hours in a nitrogen atmosphere. Zirconium nitride was obtained by nitriding zirconium hydride at 1050 ° C for 21 h [11]. A method for producing zirconium nitride by reducing zirconium oxide with carbon black in a nitrogen atmosphere at 1300 ° C is also applied. The disadvantage of this method is the presence of unreacted carbon in the products, as well as the formation of a solid solution ZrN-ZrC [12]. To obtain zirconium nitride, especially pure nitrogen is used without oxygen and water impurities [1]. Another area of industrial production is the synthesis of nitrides based on a stream of pure nitrogen which passes over the mixture [13, 14]. Additionally, it was found that the densification

mechanisms of the processed powders can be changed by electric current. The densification mechanisms depend on the particle size, temperature and pressure [1, 7, 8, 15].

Spark plasma sintering (SPS), which is also called sintering by pulsed electric current or electric field, involves the passing a pulsed DC current through a graphite matrix and using rapid Joule heating, along with uniaxial pressing. The SPS is used to obtain dense samples of nitrides. It has been established that a decrease in the yield stress of a particle material under the action of an electric current is the main mechanism for the rapid densification of conductive powders compacted with an electric current [2,15,16]. The SPS has been reported to be successful in achieving cleaner grain boundaries, improved mechanical and thermoelectric properties, improved resistance to oxidation and corrosion [1]. The SPS method has the advantage of speeding up the sintering of materials in minutes compared to the hours required to other traditional densification methods such as hot pressing or pressureless sintering [11-16].

The method for the synthesis of oxides by combustion of carbon (CCSO) [17] stimulated theoretical studies [18-23]. Models of averaging based on interpenetrating continua were proposed, in which the lost detailed information on micro-scales, such as the configuration of interphase boundaries, etc., is presented in the form of heat and mass transfer coefficients.A number of papers have shown the importance of dispersion terms in the averaged equations along with molecular diffusion of heat and matter. The concentration and the heat dispersion is caused by fluctuations in mass and heat flux, while the diffusion is caused by molecular motion. Various models of thermal dispersion have been studied in [24-30].

Modeling the synthesis of materials was developed in [18-23], in the approximation of constant pore sizes, given a priori. It should be noted that the pore sizes, as a rule, are unevenly distributed in the reactor of synthesis, the pore sizes are changed in time, affecting the fluxes of heat and the mass fluxes of reagent substances and products through the porous medium. Gradients of temperature and concentration lead to a change in volume and the appearance of displacements and stresses in the solid phase. In [31-34] models of sintering and synthesis of powder mixtures of a solid phase are considered, taking into account the mutual influence of the processes of volumetric changes in the sintering process. Thermal expansion is an important feature of a composite fuel material such as UN dispersed in ZrN.

In papers [35,36]].the effect of the concentration expansion of the solid phase under conditions of interfacial heat and mass exchange is investigated. The volumetric change in the synthesis of barium titanate BaTiO3 on the basis of a two-phase model of thermal and mass dispersion has been taken into account. A theoretical model is proposed that makes it possible to predict the characteristics of the combustion wave moving in the sample of variable porosity, when the surface type of combustion occurs. Simulation of the synthesis of barium titanate by the CCSO method in an axisymmetric SPS reactor [37], with a channel for gas supply and with an electrically conductive layer of a tungsten alloy for heating the mixture of reagents and initiating combustion, densification and sintering of the synthesis product was carried out. The themodel of thermoelasticity, thermoplasticity, and transition from elasticity to plasticity was considered. The formula of unsteady change of porosity in the synthesis zone at a given distribution of porosity at the initial moment of time is used [34]. The influence of variable porosity on the processes of synthesis of micron particles with thermal and mass dispersion accompanying convective and conductive heat - mass transfer has been studied. Concentration expansion of the gas phase due to gas pressure on the pore surface slows down the decrease in pores during combustion due to thermal and concentration expansion of the solid phase. Chemical transformations occur with a change in volume and are accompanied by the appearance of mechanical stresses and strains in addition to stresses and strains due to high temperature gradients.

In connection with the requirements of the industrial production of ceramics, there is a need to balance energy consumption, synthesis time and the quality of the final product. In this paper, we propose a model of an SPS reactor with a graphite shell of low porosity and with a gas supply through a channel specially located in the reactor close to the boundary of the synthesis zone filled with a finely dispersed reagent. A two-stage reactor for producing zirconium nitride based on the

combustion of a mixture consisting of zirconium and a nitriding agent is considered. The stream of pure nitrogen is passed over the mixture of synthesis of nitrides. The initiation of the synthesis, densification and sintering of zirconium nitride is carried out by the time-controlled Joule heat release due to an electric current passed through the tungsten channel. The degree of nitriding is controlled by the intensity of the nitrogen flow supplied at the inlet to the reactor. To simulate the synthesis of zirconium nitride, along with densification and sintering, the results of thermal and concentration expansion [33,34] and the results of thermoplasticity [38-40] are used. In the present paper modeling zirconium nitride in the reactor is considered on the basis of the macroconservation equations written in dimensionless variables including the terms of thermal and mass dispersion are presented. Simulation of the synthesis of zirconium nitride by the combustion and densification method based on the model by Olevsky [39] in an axisymmetric reactor has been carried out.The results obtained show a significant effect of volumetric changes in the solid phase.The proposed model allows us to analyze the effect of] thermal and concentration expansion on the distribution of porosity in the reactor, the synthesis rate and product distribution in the synthesis zone. This paper presents the results of modeling for particle sizes exceeding microns. Note that for micron sizes of synthesized particles, the characteristic value of the Knudsen number is small and the effects of slip and temperature jumps [41] are negligible. However, for submicron sizes of particles and pores, the influence of Knudsen layers in the gas near the pore surface becomes significant and it is necessary to take into account slip effects [18-21].

2. Theoretical analysis

2.1. Description of the model. ZrN is characterized by a wide range of stoichiometry [5, 13,42-47]. Nitriding was accompanied by a flow of N2. The application of high pressure leads to an increase the ratio of nitrogen in the powders. It is known that cold pressing with an increased load prior to the SPS process causes an increase in the contact area with the particles, which leads to a decrease in the number of open pores that affects the rapid diffusion of dissociated nitrogen pathways [1,3,4].

Let us consider the simplest scheme for the synthesis of zirconium nitride. [5.13]:

$$N_2 + 2\mathrm{Zr} \xrightarrow[Q_1]{k_1} 2\mathrm{ZrN}\,. \qquad (1)$$

The components of gas and solid phase are N_2 and $\mathrm{Zr}, \mathrm{ZrN}$. In reaction (1), the components of the solid phase do not mix at the molecular level, diffuse and move within the solid phase, k_1, Q_1 are reaction rate and the heat release in combustion of zirconium [5].

Expansion factors. The governing system of equations includes the equations of conservation of mass, energy and momentum for the gas phase and the equations of thermoelasticity and thermoplasticity based on the Duhamel - Neumann relations and the model [38] for the solid phase.

We use for the stress tensor components the generalized Duhamel - Neumann relations of the linear theory of thermoelasticity $\sigma_{ij} = 2\mu_{S1}\varepsilon_{ij} + \delta_{ij}\left(\mu_{S2}\sum_k \varepsilon_{kk} - K\omega\right)$ [48] and the relation between the invariants $\sum_k \sigma_{kk} = (2\mu_{S1} + 3\mu_{S2})\sum_k \varepsilon_{kk} - 3K\omega$ following from the Duhamel - Neumann relations, where σ_{ij} are the stress tensor components and ε_{ij} are the strain tensor components depending on the expansion coefficients, μ_{S1}, μ_{S2} are the Lane coefficients, K is the isothermal module of all-round compression. We assume that the gas pressure on the pore surface is balanced by the normal stress of the solid boundary, i.e. $\sum_k \sigma_{kk} = 3p$, then $\sum_k \varepsilon_{kk} = (K\omega + p)\mu_S^{-1}$ where $\mu_S = 2/3 \cdot \mu_{S1} + \mu_{S2}$, $\sum_k \varepsilon_{kk} = (K\omega - p)\mu_S^{-1}$. If there is no external forces then $\sigma_{ii} = 0$ and, therefore

$\sum_k \varepsilon_{kk} = K\omega\mu_S^{-1}$. Quantity $\omega = \omega_T + \omega_g + \omega_S$ is the total coefficient of volumetric expansion, in which $\omega_T = 3\alpha_T\left(-\frac{T_g}{T_g^0}+1\right)$ is the coefficient of thermal expansion, ω_g, ω_S are the coefficients of concentration expansion of the components of the gas and solid phases. The values ω_g, ω_S are estimated using the molar volumes occupied by the components $\nu_{\text{lg}} = \frac{M_{\text{lg}}}{\rho_{\text{lg}}}$, $\nu_{jS} = \frac{M_{jS}}{\rho_{jS}}$ [31, 34]. Using the molar concentrations of the components $\bar{\alpha}_{iS} = \frac{1}{3}\frac{\nu_{iS}}{\nu_{1g}+\nu_{1S}+\nu_{2S}}, i = 1,2$ we arrive at the relations $\omega_g = 0$, $\omega_g = 3\alpha_{1g}\left(-B_{1g}+B_{1g}^0\right)$ and $\omega_S = 3\left[\sum_{j=1}^{2}\alpha_{jS}\left(-B_{jS}+B_{jS}^0\right)\right]$, in which $B_{\text{lg}} = 1$, $B_{\text{lg}} = \frac{Y_{\text{lg}}}{Y_{\text{g,tot}}}$, $B_{jS} = \frac{Y_{jS}}{Y_{S,tot}}$, $B_{jS} = \frac{Y_{jS}}{Y_{1S}+Y_{2S}}$ and $Y_{jS} = \frac{\rho_{jS}}{M_{jS}}$, , the index zero refers to the values at the initial time instance.

The variable porosity of the mixture of reagents and the product for the zirconium nitrade synthesis i taking into account the effects of thermal and concentration expansion of the components of the gas and solid phases is founnd as [34]

$$\chi(t,x,r) = \frac{\chi(0,x,r)}{\chi(0,x,r)+(1-\chi(0,x,r))(1+\omega(t,x,r))}, \tag{2}$$

where $\omega(t,x,r) = \sum_{k=1}^{3}\varepsilon_{kk}(t,x,r)$. The notation $\chi(0,x,r) = \chi_0$ further is used. To simulate the effect of gas pressure on the pore surface, we introduce a scale ζ_p. Using the matching condition, we get

$$\zeta_p = -\frac{K}{P(0,\text{x},\text{r})}\left(\omega_T(0,\text{x},\text{r})+\omega_S(0,\text{x},\text{r})\right). \tag{3}$$

The governing equation of thermoplasticity for SPS. Beyond the elastic limit, the thermoplasticity model is used [48-50]. We assume that plastic deformation of the material $\dot{\gamma}$ is activated thermally, and the rate of deformation can be expressed as follows [38-40], $\dot{\gamma} = \dot{\gamma}_0 \exp\left(\frac{-E_{pl}}{RT}\right)$ where E_{pl} is the activation energy (kJ / mol), T, absolute temperature (K).

Further, the Olevsky model [38], based on the power-law plasticity, $\sigma(W) = A_m \cdot W^m$ for a porous viscous material is applied. The valur $A_m = \frac{A_0 T}{r_p}\left(\frac{d}{b}\right)^p \exp\left(\frac{-E_{pl}}{RT}\right)$, where $d = 1$, $b = 0.05$, $p = 1{,}1$, A_0, A_m are the creep coefficients for the power law, r_p is the particle size, $r_p \sim 5\cdot 10^{-7}$, T is the absolute temperature, R is the gas constant, E_{pl} is the creep activation energy according to the power law, see [38] in detail. Further we consuder $\frac{\sigma(W)}{W} = r_p A_m^m W^{m-1}$ where W is the equivalent strain rate . The densification rate $\dot{\gamma}$ and shape change $\dot{e}$ are functions of the strain rate tensor components $\dot{\gamma} = \sqrt{2\left(\dot{\varepsilon}_{xy}^2+\dot{\varepsilon}_{xz}^2+\dot{\varepsilon}_{yz}^2\right)+2/3\left(\dot{\varepsilon}_x^2+\dot{\varepsilon}_y^2+\dot{\varepsilon}_z^2\right)-2/3\left(\dot{\varepsilon}_x\dot{\varepsilon}_y+\dot{\varepsilon}_x\dot{\varepsilon}_z+\dot{\varepsilon}_z\dot{\varepsilon}_y\right)}$ [38]. The value

of the equivalent strain rate for a porous material is determined as follows $W=\frac{1}{\sqrt{1-\chi}}\sqrt{\varphi\dot{\gamma}^2+\psi\dot{e}^2}$, where $\dot{e}=\sum_k \dot{\varepsilon}_{kk}$ is the trace of the strain rate tensor.

For a power-law strain rate equivalent to creep of a porous solid, two functions of porosity are introduced: $\varphi=(1-\chi)^2$ the normalized shear modulus and $\psi=\frac{2}{3}\frac{(1-\chi)^3}{\chi}$ the normalized bulk modulus. Based on the continuous sintering theory [38-40], the constitutive equation describing hot pressing of a nonlinear-viscous porous material with a rigid matrix is expressed as: $\sigma_{ij}=\frac{\sigma(W)}{W}\left[\varphi\ \dot{\varepsilon}_{ij}+\left(\psi-\frac{1}{3}\varphi\right)\dot{e}\delta_{ij}\right]+P_L\delta_{ij}$, where σ_{ij} is the stress tensor, δ_{ij} is the unit tensor, P_L is the effective stress of free sintering, which is defined as: $P_L=\frac{3\alpha}{r_p}(1-\chi)^2$, where α a is the surface energy, r_p is the average grain diameter. In a porous medium of a gas and a solid phase, it is necessary to take into account the gas pressure at the pore boundary P_g and external pressure P_{ex}, when simulating hot pressing, along with SPS

$$\sigma_{ij}=\frac{\sigma(W)}{W}\left[\varphi\ \dot{\varepsilon}_{ij}+\left(\psi-\frac{1}{3}\varphi\right)(P_{ex}-P_g)\delta_{ij}\right]+P_L\delta_{ij}. \tag{4}$$

We consider $\dot{\varepsilon}_r=0$ [38], in this case for the rate of porosity decrease in densification, (also called the constitutive equation for nonlinear viscous densification) the following relation is valid

$$\dot{\chi}=-\left[\frac{r_p}{A_0T}\left(\frac{b}{d}\right)^p\exp\left(\frac{-E_{pl}}{RT}\right)\right]\left(\frac{3\chi}{2}\right)^{\frac{m+1}{2m}}(1-\chi)^{\frac{m-3}{2m}}\left(\frac{\sigma_{tot}}{r_p}\right)^{\frac{1}{m}},$$

where $\sigma_{tot}=P_{tot}+P_L+K\omega$.

The constitutive equation describing the densification of a nonlinearly viscous porous mixture of solid particles can be written in the form [38-40]:

$$\dot{\chi}=-A_m^{-1}\left(\frac{3\chi}{2}\right)^{\frac{m+1}{2m}}(1-\chi)^{\frac{m-3}{2m}}\left(\frac{\sigma_{tot}}{r_p}\right)^{\frac{1}{m}}. \tag{5}$$

The calculation of the change in porosity in a two-stage synthesis-densification reactor during concentration expansion based on the Duhamel-Neumn thermoelasticity relations and on the basis of the constitutive densification equation (5) was carried out using the conditional plasticity limit [48], the conditional yield strength usually means such a stress at which the permanent deformation is 0.2%. For deformation of the radius of the particle $\frac{r_P-r_P^0}{r_P^0}=0.2\%$, we obtain $\left(\frac{V_{\lim}}{V_0}\right)=8\cdot10^{-9}l_0^{-3}=10^{-3}$. Let us estimate the limiting value of porosity, taken as the plasticity limit for the particle radius $r_P\approx5\cdot10^{-7}(m)$, volume $V_P=\frac{4}{3}\pi r_P^3$. The number of particles in one mole of the mixture $n_P=N_A\cdot V_P/V_0\ \left(mol^{-1}\right)$, where Avogadro's number, $N_A=6\cdot10^{23}\ \left(mol^{-1}\right)$, $V_0=8\cdot10^{-6}$ we obtain $n_P=6\cdot10^{23}\cdot125\cdot\frac{4}{3}\pi\cdot10^{-21}\cdot10^6\ \left(m^3\cdot mol^{-1}\cdot m^{-3}\right)$, $n_P\approx1.2\cdot10^{10}$,

$\frac{V_g^{\lim}}{V_g^0}=\frac{V_g^0-V_g}{V_g^0}=10^{-3}$. Let us denote $G_0=\frac{\rho_{2s}^0}{M_{2s}}-\frac{\rho_{1s}^0}{M_{1s}}-\frac{\rho_{1g}^0}{M_{1g}}$ and $G_1=\frac{\rho_{2s}}{M_{2s}}-\frac{\rho_{1s}}{M_{1s}}-\frac{\rho_{1g}}{M_{1g}}$ the number of moles per unit volume of the mixture, then $\frac{\left(V_g^0+V_s^0\right)}{\left(V_g+V_s\right)}=V_{mol}\frac{G_1}{G_0}$, where $V_{mol}=\frac{\left(n_P\cdot V_p\right)}{\left(n_P^0\cdot V_p^0\right)}$, the index zero refers to the initial moment of time. Let $\zeta=\frac{\left(1-10^{-3}\right)\left(V_g^0+V_s^0\right)}{\left(V_g+V_s\right)}/$

If a number of moles in unit volume is not changed, i.e. $V_{mol}=1$ then we get $\zeta=\frac{\left(1-10^{-3}\right)G_1}{G_0}$.

The limiting value of porosity, according to the plasticity limit, is equal to $\chi=\zeta\chi_0$. In the computations for the range $\chi\geq\zeta\chi_0$, the thermoelasticity model and for $\chi<\zeta\chi_0$ the thermoplasticity one is used. We introduce an indicator of the thermoplasticity mode $i_{elast}(t,x,r)=\begin{cases}1, & \chi<\zeta\chi_0\\ 0, & \chi\geq\zeta\chi\end{cases}$, then for calculating the porosity we get

$$\chi(t,x,r)=\chi_1(t,x,r)\left(1-i_{elast}(t,x,r)\right)+\chi_2(t,x,r)i_{elast}(t,x,r), \tag{6}$$

$$\chi_1(t,x,r)=\frac{\chi_0\left(1+\omega_g(t,x,r)\right)}{\chi_0\left(1+\omega_g(t,x,r)\right)+\left(1-\chi_0\right)\left(1+\omega(t,x,r)\right)}, \tag{7}$$

$$\dot{\chi}_2(t,x,r)=-\left[\frac{r_p}{A_0T}\left(\frac{b}{d}\right)^p\exp\left(\frac{-E_{pl}}{RT}\right)\right]\left(\frac{3\chi_2}{2}\right)^{\frac{m+1}{2m}}\left(1-\chi_2\right)^{\frac{m-3}{2m}}\left(\frac{\sigma_{tot}}{r_p}\right)^{\frac{1}{m}}. \tag{8}$$

The dimensionless variables. We apply below the dimensionless variables, marked with a tilde as follows,

$$\tilde{x}_i=x_i/l_0\ \tilde{t}=t/t_0,\tilde{u}_i=u_i/u_0,\ \tilde{V}_{i,solid}=V_{i,solid}/u_0,\ \tilde{p}=p/p_0,u_0=l_0/t_0,\mathrm{i}=1,2,3,$$
$$\tilde{\rho}_g=\rho_g/\rho_0,\tilde{\rho}_{jg}=\rho_{jg}/\rho_0,j=1,2,3\ \tilde{c}_{pg}=C_{pg}/c_p,\tilde{c}_{pg}=C_{pg}/c_p,\tilde{D}=D/D_0,\quad \mu_0=\rho_0\nu_{air}$$
$$\rho_{1S}=\rho_{Zr},\ \rho_{2S}=\rho_{ZrN},\tilde{\rho}_{lS}=\rho_{lS}/\rho_{0Zr},\ l=1,2;\ \rho_S=\rho_{1S}+\rho_{2S}\ \tilde{c}_{pg}=C_{pg}/c_p,\ \tilde{D}_m=D_m/D_0,$$
$$\tilde{\lambda}_g=\lambda_{air}/\lambda_0,\ \tilde{\lambda}_S=\lambda_S/\lambda_0,\ \tilde{c}_S=C_S/\mathrm{c}_p,\ Ma^{-2}=\frac{\gamma_{air}p_0}{\rho_0u_0^2},\ \mathrm{Re}=\frac{l_0^2}{t_0\nu_{air}},\mathrm{R}_{Solid}=p_0\left(\zeta_p\mu_{S0}\right)^{-1},$$
$$Pe_T=\frac{l_0^2\rho_0c_p}{t_0\lambda_0},\ \ Pe_1=\frac{l_0^2}{t_0D_0},\ \tilde{Q}=\frac{Qt_0k}{\rho_0C_{pg}T_0},\ \tilde{k}=\frac{t_0k}{\rho_0},\ p_0=\frac{R\rho_0T_0}{M_0},\quad \tilde{\sigma}_{tot}=\sigma_{tot}/p_0, \tag{9}$$
$$\tilde{K}=K/\mu_{S0},\tilde{\mu}_{solid}=\mu_{solid}/\mu_{S0}\ \ \tilde{j}=j/j_0,\ j=\sigma E\ Pe_{el}=\frac{l_0^2\rho_{el}c_{p,el}}{t_0\lambda_{el}},\ R_{el}=\frac{j_0^2t_0}{l_0^2T_0\rho_0c_{p,el}}.$$
$$Pe_{gr}=\frac{l_0^2\rho_{gr}c_{p,\mathrm{gr}}}{t_0\lambda_{gr}}\ \tilde{\sigma}_{el}=\sigma_{el}/\sigma_{el,0}\ \ \tilde{E}_{el}=E_{el}/E_{el,0}.\ \tilde{\varphi}=\varphi/\varphi_0.\ \tilde{\kappa}_0=\kappa_0\,\mathrm{t}_0\mathrm{A}/\left(c_p\rho_0V\right).$$

Here $t_9=1-10(s),\ l_0=0.018\ (m)$, $A=l_0^2\ (m^2)$, $V=l_0^3\ (m^3)$, $c_p=C_{p,air}=1114(J/kg/K)$, $\rho_0=\rho_{air}=0.4(kg\cdot m^{-3}),\lambda_0=\lambda_{air}=0.06(W/m/K)$, $D_0=2\cdot10^{-5}\ (m^2/s)$, $\mu_{S0}=2\cdot10^9\ (Pa)$, $\nu_{air}=9.7\cdot10^{-5}\ (m^2/s)$, $\lambda_{el}=178\ \left(W\cdot m^{-1}\cdot K^{-1}\right)$, $Pe_{el}=0.000945$, $j_0=3500\ (A)$, $Pe_{gr}=3.132$ $\rho_{el}=1.93\cdot10^4\left(kg\cdot m^{-3}\right),c_{p,el}=24.27\left(J\cdot mol^{-1}K^{-1}\right),E_{el,0}=100\left(V\cdot m^{-1}\right),\varphi_0=l_0E_{el,0}\ (V)$, $\sigma_{el,0}=j_0/E_{el,0}\left(m^{-1}\cdot Om^{-1}\right),\ R_{el}=2\cdot10^{-7}-2\cdot10^{-5}\ \left(m\cdot Om\right),\ j_0=3500\ (A)$.

Densitie the components of the gas and solid phases as $\rho_{1g}=\rho_{N2}$, $\rho_{1s}=\rho_{Zr}, \rho_{2s}=\rho_{ZrN}$, temperature of gas and a mixture of solid components as T_g, T_S, . temperature of the graphite shell of the tungsten channel as T_{gr}, T_{el}. The temperature is found by the formula $T_{ge}=T_0\left(1+\beta\tilde{T}_{gr}\right), T_{el}=T_0\left(1+\beta\tilde{T}_{el}\right)$ $T_g=T_0\left(1+\beta\tilde{T}_g\right), T_S=T_0\left(1+\beta\tilde{T}_S\right)$. The value $\beta=RT_0/E_{comb}$ is dimensionless parameter characterizing activation energy of combustion E_{comb}, $\beta_{pl}=RT_0/E_{pl}$ dimensionless parameter characterizing activation energyof plasticity, $\beta=0.084$, $\beta_{pl}=0.05$. The values R, E, Q are the gas constant, the activation energy, the thermal effect of combustion, $p=\rho_g T_0\left(1+\beta\tilde{T}_g\right)$ is the gas pressure, κ_0 is dimensionless heat transfer coefficient, $\tilde{c}_S, \tilde{c}_{pg}$ is the heat capacity, $\tilde{\lambda}_S, \tilde{\lambda}_g$ is the thermal conductivity, the $\tilde{D}$ is diffusion coefficient, Ma, Re are the Mach and Reynolds numbers, Pe_T, Pe_1 are the thermal and diffusion Peclet numbers, the index refers to the parameters for air under normal conditions.

We present the governing equations in a form that admits a regular passage to the limit $\chi\to 0$ and $\chi\to 1$. The system of equations is presented below in dimensionless variables, the tilde symbol is omitted.

The equations of conservation of the phase density:

$$\frac{\partial\chi\rho_g}{\partial t}+\nabla\cdot\left(\chi\rho_g\,\mathbf{u}\right)=-J_{g\to S}, \frac{\partial(1-\chi)\rho_S}{\partial t}=J_{g\to S},\ J_{g\to S}=\frac{M_{1g}}{M_{1S}}J_{1S}\ . \tag{10}$$

Mass conservation equation for nitrogen component N_2

$$\frac{\partial\chi\rho_g}{\partial t}+\nabla\cdot\left(\chi\rho_g\mathbf{u}\right)=-\frac{M_{1g}}{M_{1S}}J_{1S},\ \rho_{N2}=\rho_g\ . \tag{11}$$

In reactions for the components of the solid phase, the reactants do not mix at the molecular level, diffuse and move within the solid phase. Mass conservation equation for solid phase can be written in the form

$$\frac{\partial(1-\chi)\rho_{1S}}{\partial t}=-J_{1S},\quad \frac{\partial(1-\chi)\rho_{2S}}{\partial t}=\frac{M_{2S}}{M_{1S}}J_{1S}, \tag{12}$$

where mass flux for reaction (1) is $J_{1S}=\chi^2(1-\chi)\left(\frac{\rho_{1g}}{M_{1g}}\right)^2\frac{\rho_{1S}}{M_{1S}}k_1\exp\left(\frac{T_g}{\beta T_g+1}\right)$.

The equation of gas motion in pores [18-20] is as follows.

$$\frac{\partial\chi\rho_g\,\mathbf{u}}{\partial t}+\nabla\cdot\left(\chi\rho_g\,\mathbf{uu}\right)+\mathrm{Ma}^{-2}\nabla p=\mathrm{Re}^{-1}\nabla\cdot\boldsymbol{\tau}+S_V,\ \boldsymbol{\tau}=\mu\left[\nabla\mathbf{u}+(\nabla\mathbf{u})^T-\frac{2}{3}(\nabla\cdot\mathbf{u})\mathbf{I}\right], \tag{13}$$

where the term $\mathbf{S_V}$ of the distributed gas resistance in the pores has the form $(\mathbf{S_V})_j=-u_j\eta_j$, $\eta_j=\eta_{1j}|\mathrm{u}|+\eta_{0j}$, u_j are the velocity components in the Cartesian coordinate system. $p=\rho_g\left(1+\beta T_g\right)$ is the gas phase pressure.

Let us write down the equations of motion of the solid phase in the simplest case, neglecting the influence of the work of mechanical stresses on the temperature field cp [34].

$$\frac{\partial(1-\chi)\rho_S\,\mathrm{v}_{solid}}{\partial t}+\nabla\cdot\left((1-\chi)\rho_S\,\mathrm{v}_{solid}\mathrm{v}_{solid}\right)=\mathrm{R}_{Solid}^{-1}\nabla\cdot\sigma, \tag{14}$$

$\sigma_{ij} = 2\mu_{S1}\varepsilon_{ij} + \delta_{ij}\left(\mu_{S2}\sum_k \varepsilon_{kk} - K\omega\right)$, R_{Solid} is the Reynolds number of the solid phase.

The heat balance equation for the gas phase, including dispersion, is written in the form

$$\rho_g c_{pg}\chi\left(\frac{\partial T_g}{\partial t} + \mathbf{u}\cdot\nabla T_g\right) + c_g T_g \chi J_{S\to g} = \nabla\cdot\left(\chi\frac{\mathrm{D_{Tg}}}{Pe_{Tg}}\nabla T_g\right) - \kappa\chi(1-\chi)(T_g - T_S) + \chi Q_r \,. \qquad (15)$$

The heat flux of chemical transformation $Q_r = Q_r^0\chi^2(1-\chi)\left(\frac{\rho_{1g}}{M_{1g}}\right)^2 k_1 \exp\left(\frac{T_g}{\beta T_g + 1}\right)$ is included in the right side of the equation. The thermal dispersion tensor [22] takes into account the longitudinal and transverse dispersion

$$\mathrm{D_{Tg}} = \begin{pmatrix}\lambda_{1g} & 0\\ 0 & \lambda_{2g}\end{pmatrix},\ \lambda_{1g} = \lambda_g\left(\xi + \varphi_1(Pe_{1t})\right),\ \lambda_{2g} = \lambda_g\left(\xi + \varphi_2(Pe_{2t})\right).$$

The heat balance equation for the solid phase has the form

$$\rho_S c_S(1-\chi)\left(\frac{\partial T_S}{\partial t} + \mathrm{V}_{solid}\cdot\nabla T_S\right) = \nabla\cdot\left((1-\chi)\frac{\lambda_S}{Pe_{Ts}}\nabla T_S\right) + \kappa\chi(1-\chi)(T_g - T_S) + (1-\chi)Q_r \,. \quad (16)$$

The heat transfer coefficient between the gas and solid phases is described using the Leveque formula [19,51] in the form $\kappa = \kappa_0\left(1 + \mathrm{Re}_{loc}^{0.3}\,Pe_{Tloc}^{0.3}\right)$. Here $\mathrm{Re}_{loc} = \mathrm{Re}|\mathbf{u}|\rho_g$, $Pe_{Tloc} = Pe_{Tg}|\mathbf{u}|\rho_g$ $Pe_{Tloc} = Pe_T|\mathbf{u}|\rho_g$ are the local Reynolds and Peclet numbers [19], (velocity and density are dimensionless!) $\mathrm{Re}_{loc} = \mathrm{Re}|\tilde{\mathbf{u}}|\tilde{\rho}_g$, $Pe_{Tloc} = Pe_{Tg}|\tilde{\mathbf{u}}|\tilde{\rho}_g$.

Equation of heat balance in a graphite shell is

$$\rho_{gr}c_{gr}\left(\frac{\partial T_{gr}}{\partial t}\right) = \nabla\cdot\left(\frac{\lambda_{gr}}{Pe_{gr}}\nabla T_{gr}\right) \,. \qquad (17)$$

Equation of heat balance in a tungsten channel is

$$\rho_{Wr}c_{Wr}\left(\frac{\partial T_{Wr}}{\partial t}\right) = \nabla\cdot\left(\frac{\lambda_{Wr}}{Pe_{Wr}}\nabla T_{Wr}\right) + Q_{Joul} \,. \qquad (18)$$

E-field equations based on the Ohm's law are

$$\nabla\cdot\nabla\varphi = 0\,,\quad j = \sigma E\,,\quad j = -\sigma\nabla\varphi\,,\quad E = -\nabla\varphi \,. \qquad (19)$$

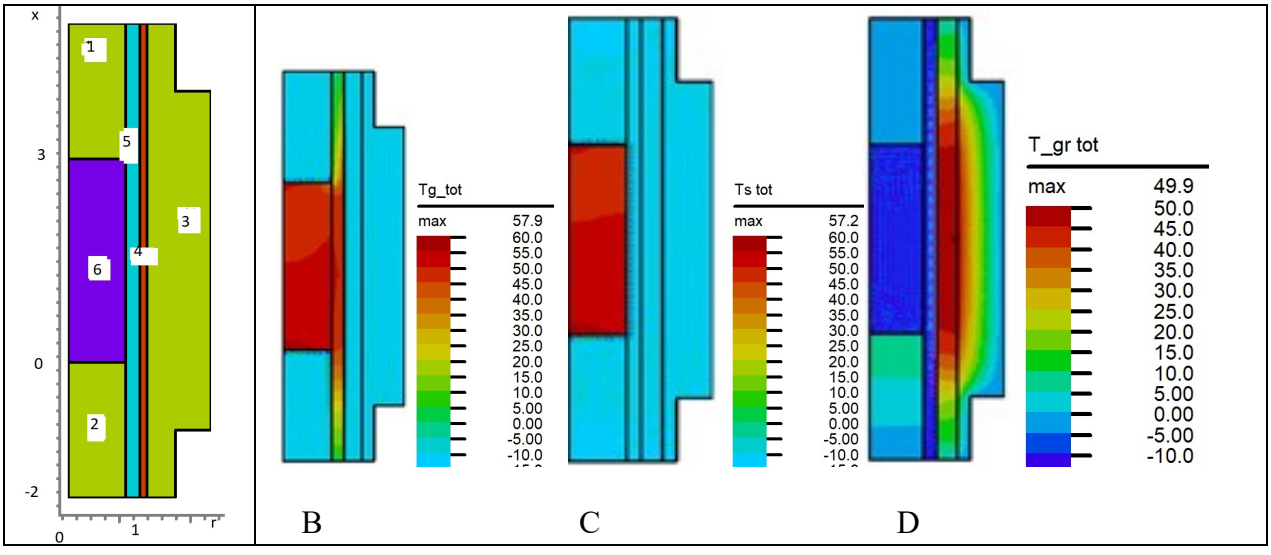

The first page (with annotation) only for English language papers

A	

Fig .. 1. Scheme of a three-zone axisymmetric reactor (Fig. 1A). The modeling area is shown, consisting of zones 1,…, 6. Zone 1: $-2 < x < 0, 0 < r < R_1$. Zone 2: $3 < x < 5, 0 < r < R_1$. Zone 3: $-1 < x < 4, 1+\delta < r < R_2$ - graphite reactor vessel. Zone 4: $-2 < x < 5, 1 < r < 1+\delta$ - tungsten layer. Zone 5: $0 < x < 3, R_1 < r < 1$ - feed channel of N_2. Zone 6: $0 < x < 3, 0 < r < R_1$ - porous area of a mixture of reagents and synthesis products. Fig. 1B and Fig. 1C illustrates the temperature distribution of the gas and the solid phase in zone 6 at time instance $t = 0.88$. Fig. 1D shows the temperature distribution of a graphite body in zones 1, 2, 3 at time instance $t = 0.88$ using a tungsten layer $-2 < x < 5, 1 < r < 1.2$.

Boundary and initial conditions. The following relations are prescribed for the reactor consisting of a synthesis region (zone A is a porous region consisted of, N_2 Zr , and ZrN). graphite body (zone B), areas of combustion of zirconium initiation consisted of tungsten alloy (zone C), channel of N_2 supply (zone d).(see Fig. 1A).

Boundary conditions at the graphite body (zones 1,2,3).

At $x = -2,\ 0 < r < 1-d;\ x = 5,\ 0 < r < 1-d;\ -2 < x < 5,\ r = 1+\delta;$ and outer boundary of zone 3 the boundary conditions are as follows

$$\frac{\partial T_{gr}}{\partial n} = \alpha_{ex}\left(T_{ex} - T_{gr}\right). \text{ At } -2 < x < 0,\ r = 1-d\ . \tag{20}$$

At $x = -2,\ 0 < r < 1-d;\ 3 < x < 5,\ r = 1-d;$ the thermal radiation / absorption condition was set according to the Stefan-Boltzmann law are imposed which in dimensionless variables has the form

$$\frac{\partial \mathrm{T}_g}{\partial n} = -q_{g,rad},\quad \frac{\partial \mathrm{T}_S}{\partial n} = -q_{S,rad},\quad q_{g,rad} = \varepsilon_\Sigma \frac{A_W}{\beta}\left(\left(1+\beta T_W\right)^4 - \left(1+\beta T_g\right)^4\right), \tag{21}$$

$q_{\mathrm{S},rad} = \varepsilon_\Sigma \frac{A_W}{\beta}\left(\left(1+\beta T_W\right)^4 - \left(1+\beta T_{gr}\right)^4\right)$, where T_{gr} is the temperature of the graphite body at the inner boundary between zones 3,4, A_W is the Boltzmann's constant in dimensionless variables $A_W = \frac{2\chi l_0^2}{r_p}\frac{\sigma_B}{\lambda_0}T_0^3$, [52]. On the inner boundary between zones 4, 5 $-2 < x < 5,\ r = 1+\delta$ the boundary condition has the form

$$\frac{\partial \mathrm{T}_{gr}}{\partial n} = -q_{gr,rad},\quad q_{gr,rad} = \varepsilon_\Sigma \frac{A_W}{\beta}\left(\left(1+\beta T_{el}\right)^4 - \left(1+\beta T_{gr}\right)^4\right). \tag{22}$$

At the boundary of zone 4 (tungsten alloy), an electric field potential $\varphi(t)$ is set, which depends on time, which makes it possible to generate electric $E(t)$ and electric current $j(t)$ and control the initiation of combustion and the thermal regime of densification of zirconium nitride. On the inner boundary between zones 4, 5 $-2 < x < 5,\ r = 1+\delta$ the boundary condition has the form

$$\frac{\partial \mathrm{T}_g}{\partial n} = -q_{g,rad},\quad q_{g,rad} = \varepsilon_\Sigma \frac{A_W}{\beta}\left(\left(1+\beta T_{el}\right)^4 - \left(1+\beta T_g\right)^4\right). \tag{23}$$

Boundary conditions at the entrance to the reactor zone 5 $x = -2, 1-d < r < 1$ are

$$\mathrm{u} = \mathrm{u}_{in},\ v = 0,\ p = p_{in},\ \frac{\partial \mathrm{T}_g}{\partial n} = -q_f(t),\ \frac{\partial \rho_g}{\partial n} = -N_{2f}\,. \tag{24}$$

Boundary conditions at the exit from the reactor zone 5 read

$$t>0;\ x=5;\ 1-d<r<1:\ \frac{\partial u}{\partial x}=0, v=0, p=p_{ex}, \frac{\partial T_g}{\partial n}=\alpha_{ex}\left(T_{ex}-T_g\right), \frac{\partial T_S}{\partial n}=\alpha_{ex}\left(T_{ex}-T_S\right). \quad (25)$$

On the inner boundaries of the zone 5 $-2<x<0,\ r=1-d$, and $-1<x<4,\ r=1$ the boundary condition has the form

$$\frac{\partial T_g}{\partial n}=-q_{g,rad}, \quad \frac{\partial T_S}{\partial n}=-q_{S,rad}, \quad q_{g,rad}=\varepsilon_\Sigma \frac{A_W}{\beta}\left((1+\beta T_W)^4-(1+\beta T_g)^4\right). \quad (26)$$

Boundary conditions for zones 1,2,6 at the axis of symmetry of the reactor $-2<x<5,\ r=0$ have the form:

$$t>0, r=0: v=0, \frac{\partial T_g}{\partial n}=0, \frac{\partial T_S}{\partial n}=0, \frac{\partial T_{gr}}{\partial n}=0. \quad (27)$$

The condition $T_S=T_g$ at the inner boundary between the channel and zone 6, $0<x<3,\ r=1-d$ if imposed, ∂/∂n denotes the normal derivative, $R_1=1-d$.

Initial conditions $t=0$, $u=0, v=0$, $T_g=T^0$, $T_S=T^0$, $T_{gr}=T^0$, $T_{el}=T^0$

$$T_g=T^0,\ T_S=T^0\ t=0;\ 0<x<3;\ 0<r<1-d:\ u=u^0, v=0, \rho_g=\rho_g^0,\ \rho_{jS}=\rho_{jS}^0\ j=1,2, \quad (28)$$

where the superscript zero refers to the value of the variable at the initial time.

The finite element method tested in our previous papers [10-23] has been applied. The results of simulation were validated using various meshes. The results of numerical solution of equations (10) - (19) with relations (6)-(8), (20)-(28) are presented in Fig. 1- Fig. 10.

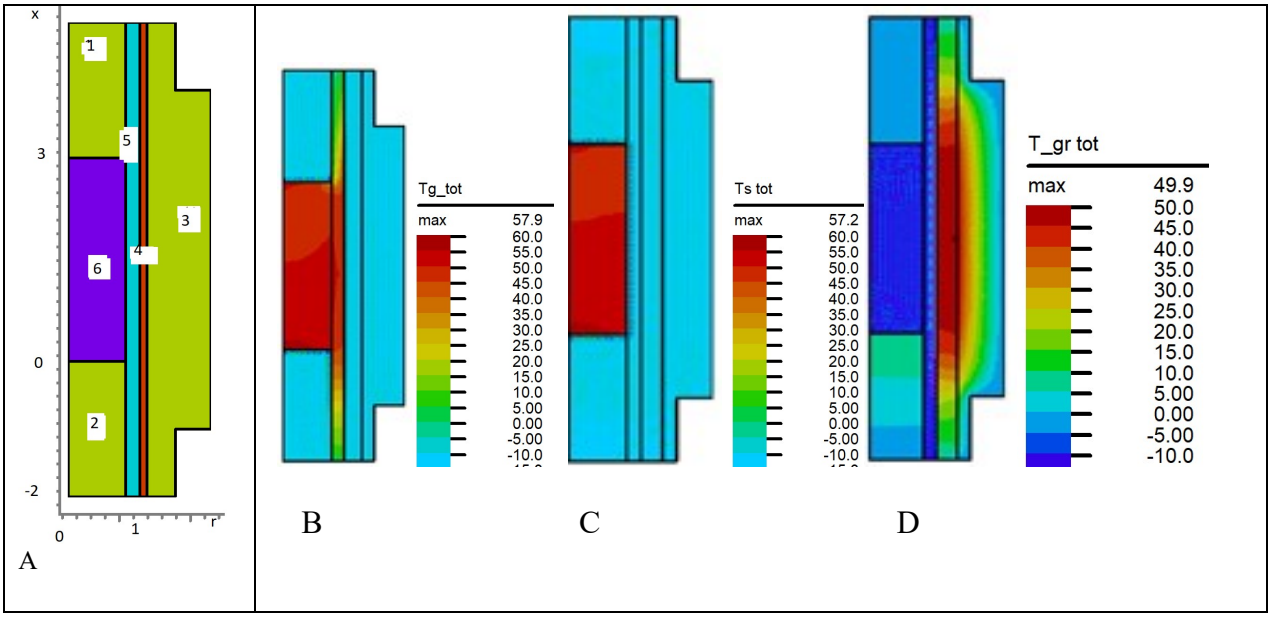

Fig 1. Schematic of the SPS reactor. Zone A: - porous region of a mixture of gas, reagent Zr and product of ZrN synthesis. Zone B, consisting of three parts B1: -2 <x <0, B: 2 and B3: - graphite body. Zone C - area of initiation of combustion of zirconium in nitrogen Zone d: - feed channel. (Fig. 1A). In Fig. B and FIG. B1 illustrates the distribution and scale of the temperature of the solid phase at a point in time. FIG. C and FIG. C1 shows the distribution of porosity at the moment of time, Hi_ex = 1e-6.

The first page (with annotation) only for English language papers

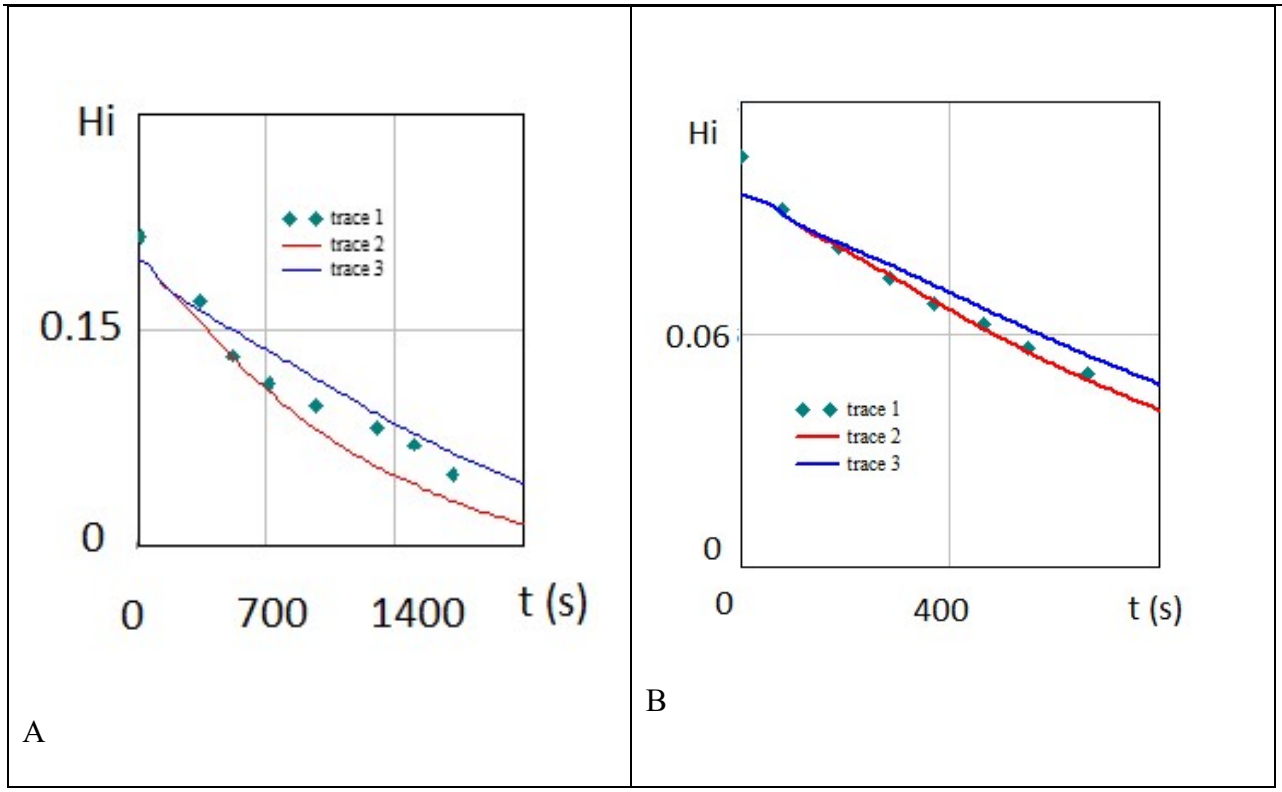

Fig. 2 demonstrates the comparison with experiment. The comparison of porosity with experiment [16] for $r_p = 1.2 \cdot 10^{-5}, m = 0.33, A_0 = 4.3 \cdot 10^{-9} \left(Pa \cdot s \cdot K^{-1} \right)$ and $r_p = 8.5 \cdot 10^{-6}, m = 0.36$, $A_0 = 5.4 \cdot 10^{-9} \left(Pa \cdot s \cdot K^{-1} \right)$, see (8) is shown in fig. 2B for temperature rise with rate $10\,C/\min$. Symbols 1 refer to $SPS, T = 1100(C)$,Fig. 2A and $SPS, T = 1200(C)$, Fig. 2B respectively, $t_9 = 10(s)$. Solid lines 2.3, in Fig. 2A refer to porosity at points with coordinates(0.9,0.5), (1.42,0.5) and lines 2,3 in Fig. 2B refer to porosity at points with coordinates (0.9,0.75), (2.14,0.75).

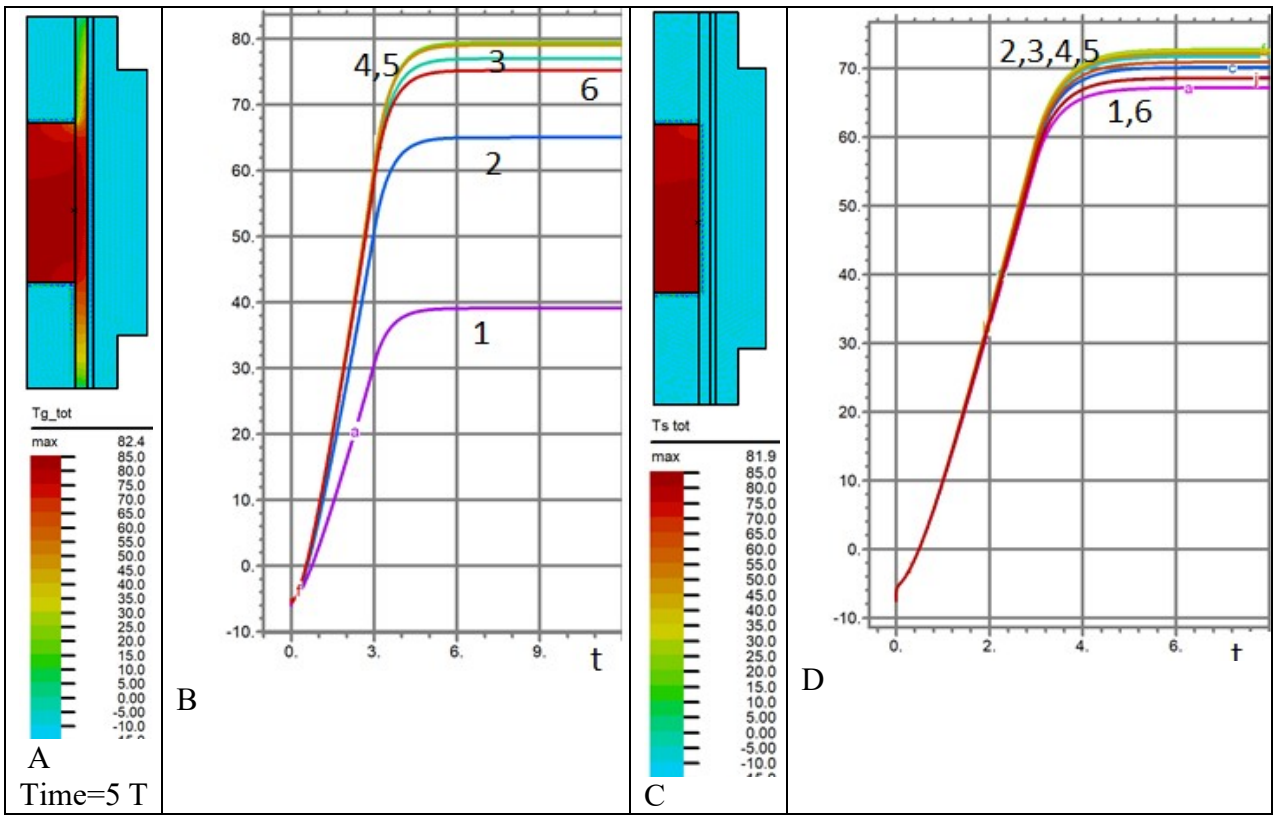

		Time=5	

Fig. 3 Shows the gas temperature (Fig. 3A, Fig. 3B) and the temperature of the solid phase (Fig. 3C, Fig. 3D). In fig. 3A, Fig. 3C illustrates the field Tg (t, x, r), Ts (t, x, r) t = 5, Fig. 3B, Fig. 3D illustrates the Tg and Ts dynamics. Lines 1,…, 6 refer to points (x, r) with coordinates; (0,0.75) (0.14,0.75) ,(0.9,0.75), (1.42,0.75), (2.14,0.75), (2.86,0.75) respectively.

The change in gas temperature in Fig. 3B and solid phase temperatures in Fig. 3D demonstrates the dynamics of heating and the degree of nonequilibrium, which follows from the difference between Tg and Ts near the boundary 0 <x <3, r = 0.8.

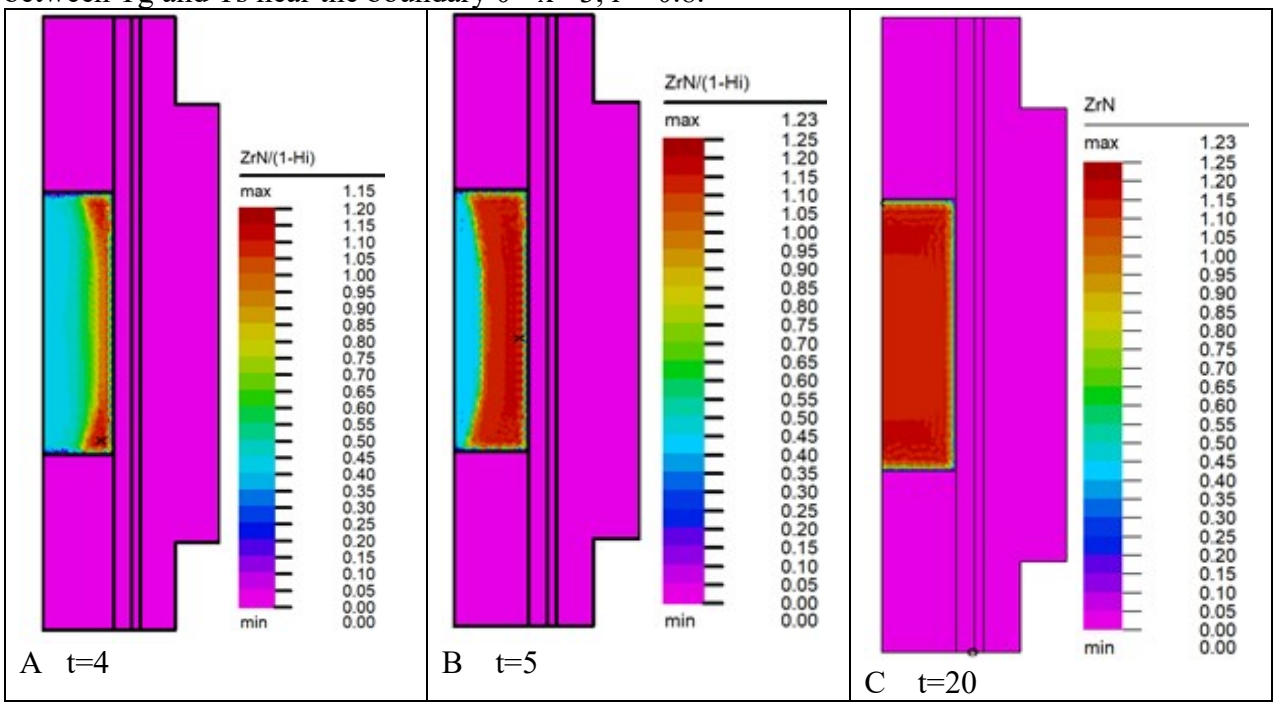

Fig 4. The dynamics of the synthesis of zirconium nitride is illustrated. In fig 4A, fig. 4B and Fig. 4C shows the field $ZrN(t,x,r)$ at time instances t = 4, t = 5, and t = 20, respectively.

The dynamics of the synthesis of zirconium nitride shown in Fig. 4A, Fig. 4B, Fig. 4C, demonstrates the degree of inhomogeneity of the $ZrN(t,x,r)$ distribution at t = 4 and t = 5. By the time t = 20, the distribution of $ZrN(t,x,r)$ is close to uniform, with the porosity $\chi_{ex}=5\cdot10^{-4}$ of the graphite body.

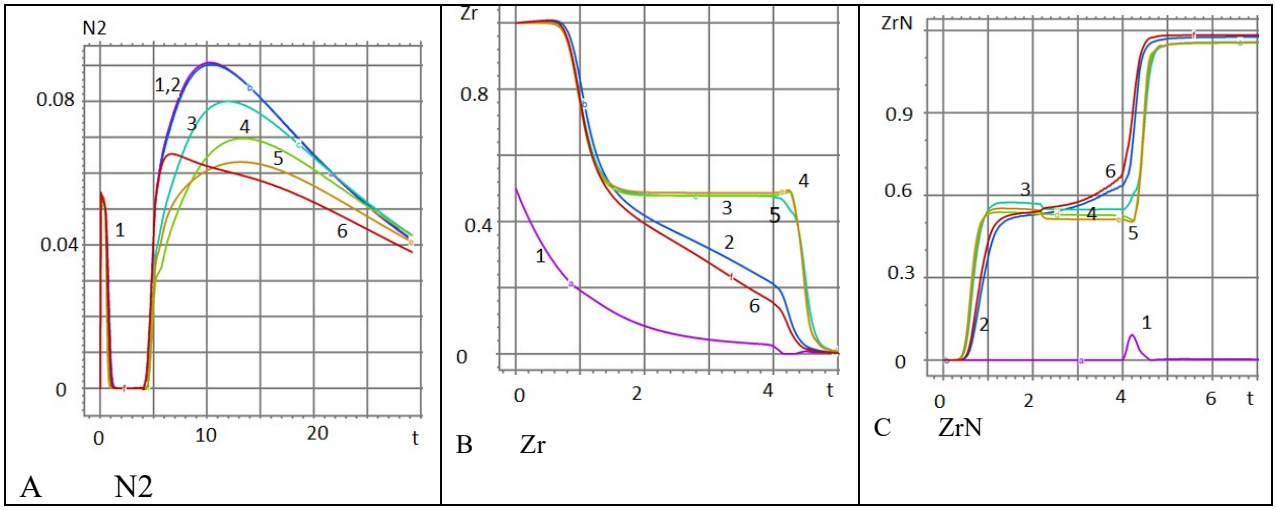

The first page (with annotation) only for English language papers

The dynamics of nitrogen, zirconium and zirconium nitride in a two-stage nitrogen supply mode is illustrated. The fig 5A, fig. 5B and Fig. 5C show the time variation of N_2, Zr and ZrN, respectively, at points with coordinates (0,0.5) (0.14,0.5) ,(0.9,0.5), (1.42,0.5), (2.14,0.5), (2.86,0.5).

Fig. 5 shows the effect of the two-stage nitrogen supply at time intervals: $N_{2f}=1,\ 0<t<0.2$ and , $N_{2f}=0,\ 0.2<t<5$, and $t>10$. The time history of the density N2 at points with coordinates (1 / 7,0.5), (5 / 77,0.5), (10 / 7,0.5), (15 / 7,0.5), (20/7 , 0.5) is shown in Fig. 5A. Note the deficit of the reagent N2 in the time interval 0, 0.2 <t <5, leading to a zone of constant distribution of Zr and ZrN densities lines 3,4,5 in Fig. 5B and Fig. 5C.

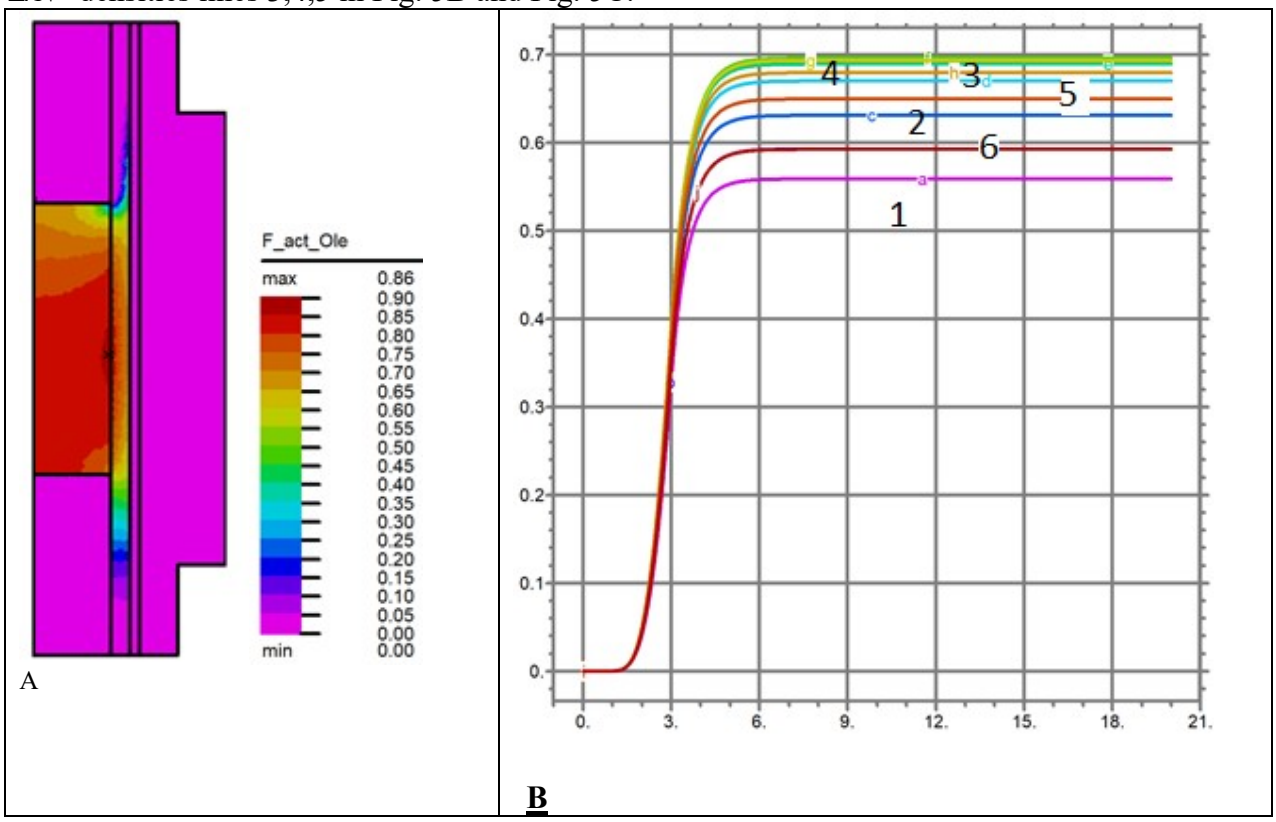

Fig. 6 presents the activation energy $A_m(t,x,r)$ of the densification process in the Olevsky model.The field $A_m(t,x,r)$ is shown in Fig. 6A, ar time instance $t=10$. The time history of $A_m(t,x,r)$ at points with coordinates(0,0.8) (0.14,0.8) ,(0.9,0.8), (1.42,0.8), (2.14,0.8), (2.86,0.8), lines 1,…,6 respectively is shown in Fig. 6B.

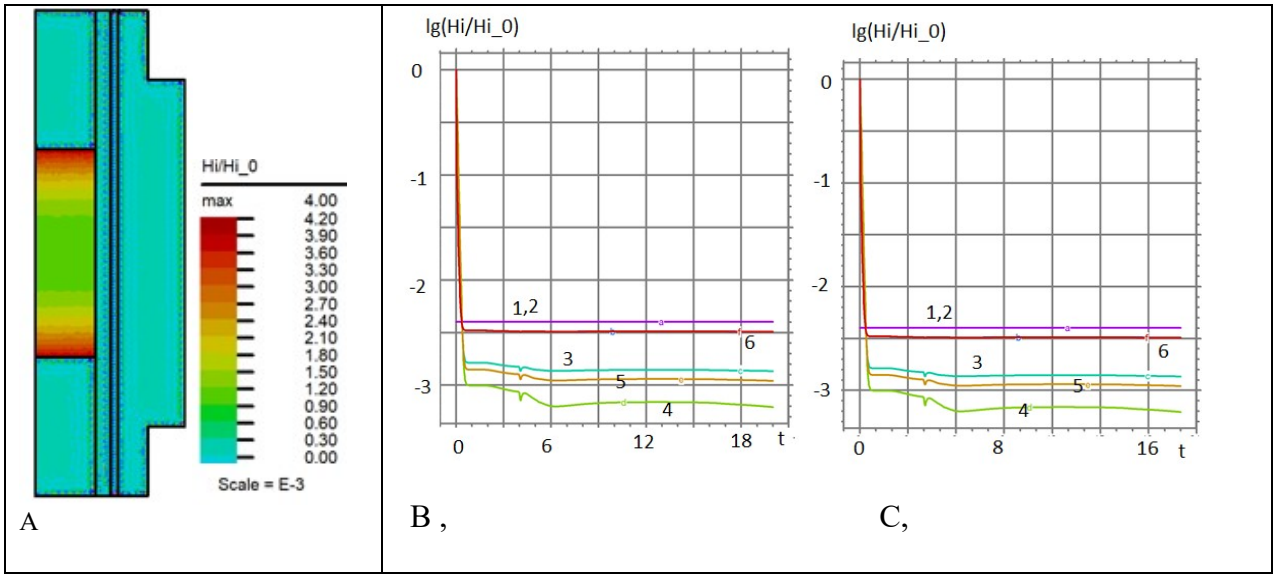

Fig. 7. The porosity of the solid phase $r_p = 5 \cdot 10^{-7}$ in the densification process is shown according to the model (2) and (5) .. In Fig. 7A, the $\chi(t,x,r)/\chi_0$ ratio of the porosity at the time instance t to the initial porosity is given. In fig. 7B and Fig. 7C shows the change in time of the decimal logarithm $\lg(\chi(t,x,r)/\chi_0)$ at points with coordinates (0,0.75) (0.14,0.75) ,(0.9,0.75), (1.42,0.75), (2.14,0.75), (2.86,0.75) and (0,0.) (0.14,0.) ,(0.9,0.), (1.42,0.), (2.14,0.), (2.86,0.) respectively.

Fig. 7. shows the densification process in the time interval 0 <t <20, fig. 7B and Fig. 7C. Figure 7A shows the ratio of the porosity at time to the initial porosity $\lg(\chi(t,x,r)/\chi_0)$. The porosity of the solid phase during densification was calculated according to the model (2) and (5). Fig.7A $\chi(t,x,r)/\chi_0$ at time instance t=40. The rime history $\lg(\chi(t,x,r)/\chi_0)$ at points with coordinates (0,0.75) (0.14,0.75) ,(0.9,0.75), (1.42,0.75), (2.14,0.75), (2.86,0.75) for $\chi_{ex} = 5 \cdot 10^{-4}$ is presented in Fig. 7B and Fig. 7C.Note the value $\chi(t,x,r)/\chi_0$ are three orders of magnitude, lines 3,4,5 in Fig. 7B and Fig. 7C. Slower densification occurs near the boundary of the synthesis zone with graphite whose porosity is $\chi_{ex} = 5 \cdot 10^{-4}$ see Figure 7A and line 1.6 in Figure 7B and Figure 7C.

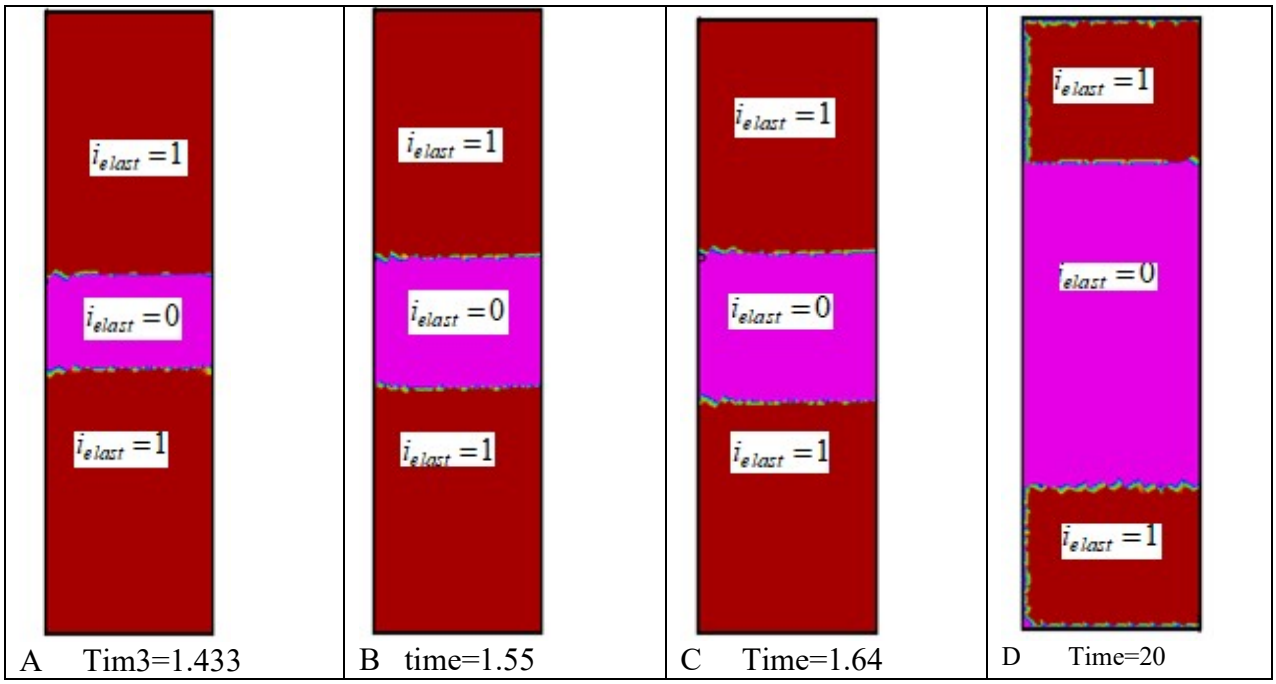

Fig. 8. The dynamics of the zones of densification are illustrated by the thermoelasticity model $i_{elast}(t,x,r)=1$ and the thermoplasticity mode $i_{elast}(t,x,r)=0$ l.In fig 8A, fig. 8B, Fig. 8C and Fig. 8D shows the zones at times t = 1.43, t = 1.55, t = 1.64 and t = 20, respectively.

Figure 8 shows the dynamics $i_{elast}(t,x,r)$ for. $\chi_{ex} = 10^{-3}$ Note the expansion of the zone of $i_{elast}(t,x,r)=0$ thermoplastic properties of ZrN in the middle of the synthesis region and a decrease in the size of the zone $i_{elast}(t,x,r)=1$ in which the thermoelastic properties of ZrN are manifested at moments. time t t = 1.43, t = 1.55, t = 1.64 and t = 20 in Fig.8A, Fig. 8B, Fig. 8C and Fig. 8D.

The first page (with annotation) only for English language papers

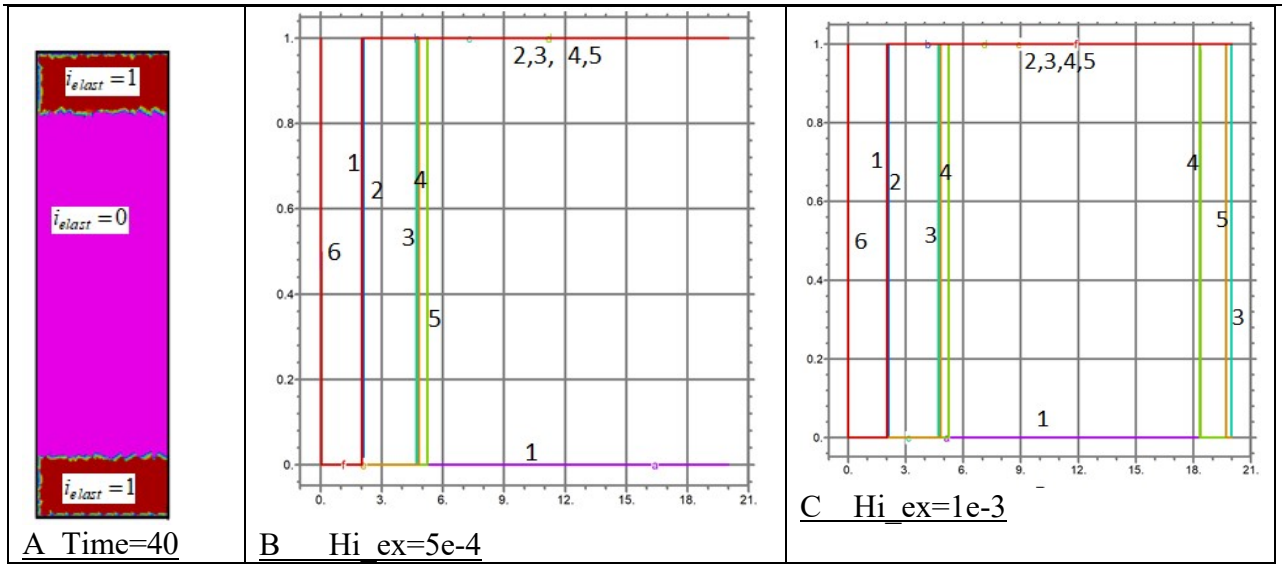

Fig. . 9. The zones of densification $i_{elast}(t,x,r)=1$ are given according to the thermoelasticity model and the thermoplasticity mode $i_{elast}(t,x,r)=0$ l for external porosity $\chi_{ex}=5\cdot10^{-4}$ and $\chi_{ex}=10^{-3}$. Figure 9A shows the zones at times t = 40, $\chi_{ex}=5\cdot10^{-4}$. Fig. 9B, and Fig. 9C show the dynamics of the zones at $\chi_{ex}=5\cdot10^{-4}$ and $\chi_{ex}=10^{-3}$, respectively. The time history of the value $i_{elast}(t,x,r)=1$ at points with coordinates is illustrated: (0,0.) (0.14,0.) ,(0.9,0.), (1.42,0.), (2.14,0.), (2.86,0.), lines 1,2, ..., 6, respectively.

As you can see from fig. 9A, by the time t = 40, the region of thermoplastic change in the solid phase prevails in the reactor. The thermoelastic properties of the solid phase, which at this time is almost entirely composed of zirconium nitride, appear in the regions near the boundaries of the reactor: x = 0, 0 <r <0.8 and x = 3, 0 <r <0.8 (see Fig.1A). Tracing the dynamics $i_{elast}(t,x,r)$ for $\chi_{ex}=5\cdot10^{-4}$ at points with coordinates: (5 / 77.0), (10 / 7.0), (15 / 7.0), (20 / 7.0), lines 2,3, ..., 6, shown in fig. 9B, we note that having arisen at points in time with a zero ordinate of points on lines 2, ..., 6, the thermoplastic properties of *ZrN* change to thermoelastic properties, and these properties are inherent in *ZrN* at all subsequent moments. time t <21. Note the difference in the dynamics of the thermoplastic and thermoelastic properties of *ZrN* in the case of the higher porosity of the graphite shell, Fig. 9C. The difference from the case considered above is that, having arisen at times with a zero ordinate of points on lines 2, ..., 6, the thermoplastic properties of *ZrN* change to thermoelastic properties, which are again replaced by thermoplastic ones at t> 18.

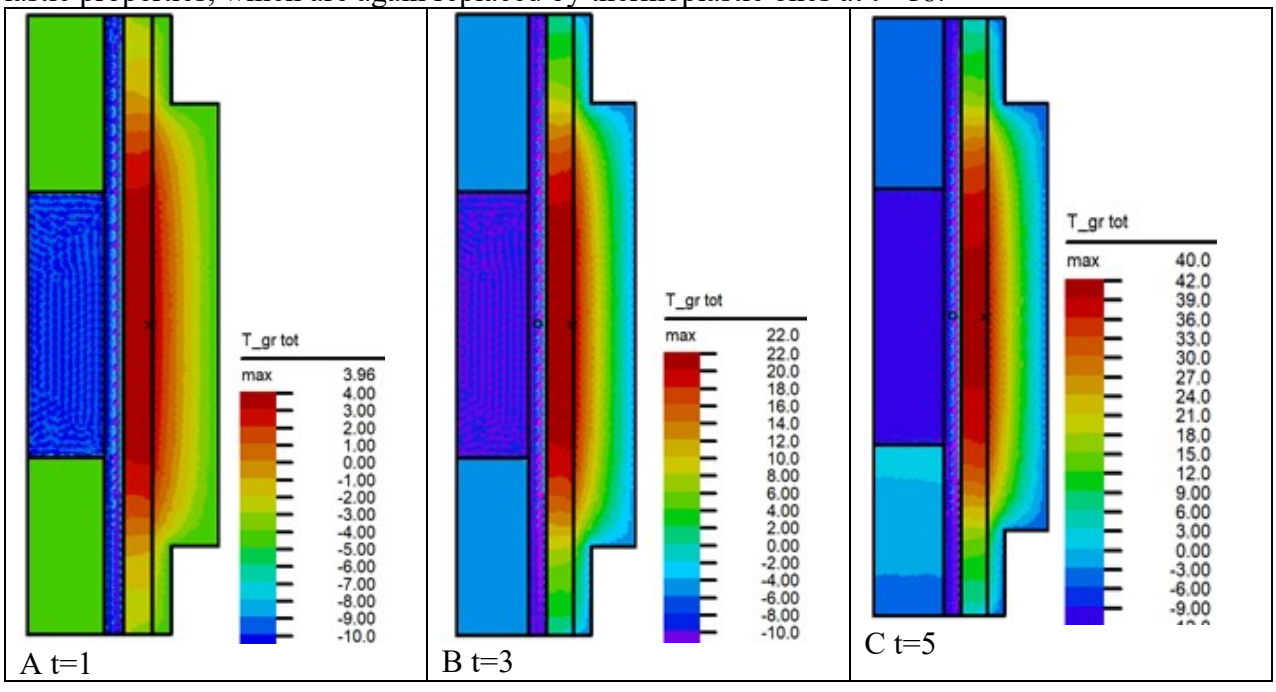

Fig. 10. Dynamics of heating the graphite body for the thickness of region 5 (Fig. 1) Delta_r = 0.3. In fig 10A, fig. 10B and Fig. 10C shows the T_gr (t, x, r) field at times t = 1, t = 3, and t = 5, respectively.

The heating of the graphite shell at a given increase in the electric field strength $E(t)=\sqrt{0.5\cdot t}, 0<t<34$ and $E(t)=0,\ t\geq 4$ is presented by the temperature distributions T_gr (t, x, r) at times t = 1, t = 3 and t = 5 in Fig. 10A, Fig. 10B and Fig. 10C respectively. Note the maximum values of T_gr = 4, 22, and 42. at times t = 1, t = 3, and t = 5

Conclusion

The investigation of the synthesis and densification of zirconium nitride was carried out using the proposed model of multitemperature reactor, which differs from the typical model of the SPS reactor [38-40] by the presence of a gas flow channel and an specifically located electrically conductive tungsten alloy layer. The study of volumetric changes and variable porosity during the densification of the solid phase in the synthesis of zirconium nitride is presented. The reactor allows us to to analyze the stages of synthesis and sintering processes. A generalization of the two-temperature model [33, 37] and a variable porosity formula are proposed for self-consistent calculation of the multitemperature heat transfer in the reactor. The computation including thermal radiation, concentration expansion, thermal and mass dispersion are carried out The coefficients of concentration expansion are found in the process of zirconium combustion in the porous zone of the reactor, depending on the kinetics of synthesis of zirconium nitride at given initial values of gas and solid phases for unsteady nitrogen supply through gas channel. The approach allows us to control the rate of nitriding.

The effect of electric current on spark plasma densification and sintering (SPS) of ZrN powder was investigated. The thermoplasticity constitutive equation [38] was applied, taking into account the effect of electric current and generalization of the porosity formula [33] for calculating the thermoelastic properties of the solid phase during the synthesis and densification of ZrN. The temperature inside the mixture of zirconium powder with synthesized zirconium nitride, the temperature of the gas phase (N2) and the temperature of the porous graphite shell of the reactor at a given electric potential applied to the electrodes of the tungsten layer and a given variation in time the electric current density is simulated. A model of the elastic limit for a porous mixture of solid particles with a gas phase is proposed, using the elastic limit for a solid spherical particle, the particle size and the particle number density. Calculations of the densification of zirconium nitride with the separation of zones in which the thermoelastic and thermoplastic properties of the solid phase prevail for the average particle size of 5e-7 have been carried out. A decrease in porosity by three orders of magnitude compared to the initial value is demonstrated. The influence of the low porosity of the graphite shell of the SPS reactor on the dynamics of densification is considered.

Estimation of volumetric deformations. arising as a result of a change in the temperature and concentration of a mixture of reagents and a product of ZrN during synthesis were caried out. The controlled Joule heating by electric current in a conducting layer, allows to conclude that the temperature change during synthesis and densification strongly depends on the initial phase composition and effects the final ZrN distribution in the sample, its volume as well as the duration of the process.

The performed modeling of the synthesis and densification of ZrN indicates an uneven distribution of thermoelastic, thermoplastic properties, and porosity of ZrN in the reactor. The results obtained demonstrate a significant effect of variable porosity on the synthesis of fine ZrN particles. The ZrN densification mechanism can be changed through enhanced movement of dislocations due to local resistive heating. [1].

The developed model of the SPS reactor with a gas flow and an electrically conductive layer can be applied for other materials subjected to sintering using an electric field [1,38].by adjusting the parameters to appropriate data of experiments .

Author acknowledges support in the framework of governmental program for IPMech RAS topic no AAAA-A20-120011690135-5.

Refferences

[1] R. W. Harrison & W. E. Lee (2016) Processing and properties of ZrC, ZrN and ZrCN ceramics: Advances in Applied Ceramics, 115:5, 294-307, DOI: 10.1179/1743676115Y.0000000061.
[2] Z. A. Munir, U. Anselmi-Tamburini and M. Ohyanagi: 'Theeffect of electric field and pressure on the synthesis and consolidation of materials: a review of the spark plasma sintering method, J', Mater. Sci., 2006, 41, (3), 763–777.
[3] D. M. Hulbert, A. Anders, J. Andersson, E. J. Lavernia and A. K. Mukherjee: 'A discussion on the absence of plasma in spark plasma sintering', Scr. Mater, 2009, 60, (10), 835–838.
[4] H. F. Jackson and W. E. Lee: 'Properties and characteristics of ZrC', in 'Comprehensive nuclear materials', (ed. R. J. M. Konings), 339–372; 2012, Oxford, Elsevier.
[5] Shijiao Zhao, Jingtao Ma, Rui Xu, Xuping Lin, Xing Cheng, Shaochang Hao, Xingyu Zhao, Changsheng Deng, Bing Liu·Synthesis and Characterization of Zirconium Nitride Nanopowders by Internal Gelation and Carbothermic Nitridation.// CIENTIFIC REPORTS | *(2019)9:19199* | https://doi.org/10.1038/s41598-019-55450-x
[6] Dietz A.A. Oxynitride ceramic materials based on combustion products of industrial metal powders in air. // Dissertation. Tomsk 2006
[7] Russias, S. Cardinal, C. Esnouf, G. Fantozzi and K. Bienvenu: 'Hot pressed titanium nitride obtained from SHS starting powders: influence of a pre-sintering heat-treatment of the starting powders on the densification process', J. Eur. Ceram. Soc., 2007, 27(1), 327-335.
[8] T. Sakai and M. Iwata: 'Effect of oxygen on sintering of AlN',J. Mater. Sci, 1977, 12, (8), 1659–1665.
[9] Z. A. Munir, U. Anselmi-Tamburini and M. Ohyanagi: 'Theeffect of electric field and pressure on the synthesis andconsolidation of materials: a review of the spark plasmasintering method, J', Mater. Sci., 2006, 41, (3), 763–777.
[10] Merja, P., Masahide, T. 8c Tsuyoshi, N. Sintering and characterization of (Pu,Zr)N. J. Nucl. Mater. 444,421-427 (2014).,.
[11] G.V. Samsonov Nitrides / ed. E.E. Gritsenko. - Kiev: Naukova Dumka, 1969 .-- 379 p.
[12] Kurganov G.V., Levinsky Yu.V. et al. Chemistry and Physics of Nitrides / G.V. Kurganov and others - Kiev: Naukova Dumka, 1968 .-- 47 p.
[13] R. Harrison, O. Rapaud, N. Pradeilles, A. Maitre and W. E. Lee: 'On the fabrication of ZrCxNy from ZrO2 via two-step carbothermic reduction-nitridation', J. Eur. Ceram. Soc, 2015, 35, (5), 1413-1421.
[14] G.V. Samsonov Nitrides / ed. E.E. Gritsenko. - Kiev: Naukova Dumka, 1969 .-- 379 p.
[15] G. Lee, M.S. Yurlova, D. Giuntini, E.G. Grigoryev, O.L. Khasanov, J. McKittrick, E.A. Olevsky, Densification of zirconium nitride by spark plasma sintering and high voltage electric discharge consolidation: A comparative analysis, Ceram. Int. 41(10, Part B) (2015) 14973-14987.
[16] G. Lee, E.A. Olevsky, C. Maniere, A. Maximenko, O. Izhvanov, C. Back, J. McKittrick, Effect of electric current on densification behavior of conductive ceramic powders consolidated by spark plasma sintering, Acta Materialia (2017), doi: 10.1016/j.actamat.2017.11.010.)
[17] Martirosyan K S and Luss D. Carbon Combustion Synthesis of Oxides Process Demonstration and Features *AIChE* 2005, vol. J 51 10, pp. 2801-2810.
[18] A.A. Markov, M.A. Hobossian, K.S. Martirosyan. Investigation of the synthesis of ferrites behind the combustion wave using models of sliding and temperature jumps and concentrations of the components of the gas phase on the surface of the pores of the solid phase. Physicochemical kinetics in gas dynamics 2015 V16 (1)
[19] A.A. Markov, I.A. Filimonov, and K.S. Martirosyan, Synthesis simulation of submicron particles of complex oxides // Theoretical Foundations of Chemical Engineering 2017(1) pp.1-12.
[20] Markov, I. A. Filimonov, and K. S. Martirosyan. Carbon Combustion Synthesis of Oxides:

Effect of Mach, Peclet, and Reynolds Numbers on Gas Dynamics. International Journal of Self Propagating High Temperature Synthesis, 2013, 22, No. 1, pp. 11–17.
[21] A.A. Markov, I.A. Filimonov, and K.S. Martirosyan. Simulation of front motion in a reacting condensed two phase mixture, J. Comput. Phys. Volume 231, Issue 20, 15 August 2012, Pages 6714–6724 (2012).
[22] A.A. Markov, On Thermal and Mass Dispersion Effect on Barium Titanate Synthesis via CCSO. *Physical-Chemical Kinetics in Gas Dynamics* 2019 V20 (4) pp. 1-14. http://chemphys.edu.ru/issues/2019-20-4/articles/870/, http://www.chemphys.edu.ru DOI: http://doi.org/10.33257/PhChGD.20.4.870
[23] A A Markov. On fine particles synthesis using three-zone reactor August 2020. Journal of Physics Conference Series 1611:012047. DOI: 10.1088/1742-6596/1611/1/012047
[24] Whitaker S Transport equations for multi-phase systems Chemical Engineering Science,1973 vol 28 pp 139-147
[25] Hsu, C.T.; Cheng, P.: Thermal dispersion in a porous medium. Int. J. Heat Mass Transf. 1990 33, 1587–1597.
[26] Fatehi M and Kaviany M Role of gas-phase reaction and gas-solid thermal nonequilibrium in reverse combustion Int Heat Mass Transfer 1997 11 pp 2607-20
[27] Oliveira A A M and Kaviany M Nonequilibrium in the transport of heat and reactants in combustion in porous media Progress in Energy and Combustion Science 2001 27 pp 523-45
[28] F. M. Pereira, A. A. M. Oliveira and F. F. Fachini. Theoretical analysis of ultra-lean premixed flames in porous inert media J. Fluid Mech. 2010, 657, pp. 285–307.
[29] M. Fatehi and M. Kaviany. Role of gas-phase reaction and gas-solid thermal nonequilibrium in reverse combustion. Int. Heat Mass Transfer. 1997 11, pp.2607-2620.
[30] Delgado JMPQ 2007 Longitudinal and transverse dispersion in porous media Chem Eng Res Des 2007 85 pp 1245–1252
[31] S.N. Sorokova, A.G. Knyazeva. Associated model of sintering powders of the Ti-TiAI3 system // Bulletin of the Tomsk Polytechnic University. 2009. T. 314. No. 2. S. 96-101.
[32] S.N. Sorokova, A.G. Knyazeva. Mathematical modeling of volumetric changes during sintering of powders of the Ti-Al system. // Physical mesomechanics 11 6 (2008) 95-101.
[33] Markov, A.. Modeling the Synthesis of Barium Titanate Micron Particles in Axisymmetric Direct-Flow and Three-Zone Reactors. *J Eng Phys Thermophy* **94,** 1312–1325 (2021). https://doi.org/10.1007/s10891-021-02412-8
[34] A. A. Markov. Thermal and Concentration Expansion in the Synthesis of Barium Titanate in a Once-Through Reactor.// Theoretical Foundations of Chemical Engineering, 2021, Vol. 55, No. 5, pp. 929–941.
[35] J. Adachi, K. Kurosaki, M. Uno and S. Yamanaka: 'Thermal and electrical properties of zirconium nitride', J. Alloys Compd, 2005, 399, (12), 242–244.
[36] K. Aigner, W. Lengauer, D. Rafaja and P. Ettmayer: 'Lattice parameters and thermal expansion of Ti(CxN^x), Zr(CxN^x), Hf(CxN1.x) and TiN^x from 298 to 1473 K as investigated by high-temperature X-ray diffraction', *J. Alloys Compd,* 1994, 215, (1-2), 121-126.
[37] A.A. Markov. Simulation of a two-stage reactor for the synthesis and sintering of ultrafine zirconium nitride. // Proceedings of the Twenty-second International Conference on Computational Mechanics and Modern Applied Software Systems (VMSPS'2021), September 4-13, 2021 Alushta, -. M. Publishing house MAI, pp. 411-413. ISBN 978-5-4316-0824-7.(in Russian).
[38] Olevsky E.A. (1998), Theory of sintering: from discrete to continuum. Review, Mater. Sci. & Eng. R: Reports, 40-10
[39] E. Olevsky, G. Timmermans, M. Shtern, L. Froyen, and L. Delaey, The permeable element method for modeling of deformation processes in porous and powder materials: Theoretical basis and checking by experiments, *Powd. Technol.* -93/2, 123-141 (1997)
[40] E. Olevsky, V. Tikare, and T. Garino, Multi-scale modeling of sintering - A Review, *J. Amer. Ceram. Soc.,* 89 (6), 1914-1922 (2006)
[41] Markov A. A. Jump-Slip simulation technique for combustion in submicron tubes and

submicron pores. Computers and Fluids 2014 99C, pp. 83-92.
[42] R. Harrison, O. Rapaud, N. Pradeilles, A. Maitre and W. E. Lee: 'On the fabrication of ZrCxNy from ZrO2 via two-step carbothermic reduction-nitridation', J. Eur. Ceram. Soc, 2015, 35, (5), 1413-1421.
[43] Xie, Z. Fu, Y. Wang, S. W. Lee and K. Niihara: 'Synthesis of nanosized zirconium carbide powders by a combinational method of sol-gel and pulse current heating', J. Eur. Ceram. Soc, 2014, 34, (1), 13e1-13e7.
[44] Bardelle and D. Warin: 'Mechanism and kinetics of the uranium-plutonium mononitride synthesis', J. Nucl. Mater, 1992, 188, 36^2.
[45] Merja, P., Masahide, T. 8c Tsuyoshi, N. Sintering and characterization of (Pu,Zr) N. J. Nucl. Mater. 444,421-427 (2014).
[46] A. Ortega, M. D. Alcala and C. Real: 'Carbothermal synthesis of silicon nitride (Si3N4): kinetics and diffusion mechanism', J. Mater. Process. Technol., 2008, 195, (13), 224-231.
[47] A. W. Weimer, G. A. Eisman, D. W. Susnitzky, D. R. Beaman and J. W. McCoy: 'Mechanism and kinetics of the carbothermal nitridation synthesis of alpha-silicon nitride', J. Am. Ceram. Soc, 1997, 80, (11), 2853-2863.
[48] Bruno A. Boley, Jerome H. Weiner.Theory of Thermal Stresses (Dover Civil and Mechanical Engineering) Revised Edition. Publisher : Dover Publications; Revised edition 2011. 608 p.
[49] H. Conrad, Electroplasticity in metals and ceramics, Mat. Sci. Eng. A. 287(2) (2000) 276- 287
[50] B. A. Boley, J. H. Weiner, Theory of Thermal Stresses, Dover Publications, p. 608, 2011.
[51] D.A. Frank-Kamenetskii, Diffusion and Heat Transfer in Chemical Kinetics (Second Enlarged and Revised Edition), Translation Editor: J.P. Appleton, Plenum Press, 1969.
[52] A A Markov and I A Filimonov. Model of thermal radiation using heat absorption by CO2 in submicron pores with application to magnesium-zinc ferritefine disperse particles synthesis via combustion // APhM2017 IOP Publishing IOP Conf. Series: Journal of Physics: Conf. Series **1009** (2018) 012040 doi :10.1088/1742-6596/1009/1/012040.

List of principal notations

T_0	Referred temperature (K)
T'	Dimensional temperature
$T=\frac{T'}{T_0}$	Dimensionless temperature
$\tilde{T}=\frac{T-1}{\beta}$	Dimensionless normalized temperature
T_g, T_{jS}	Gas temperature and solid phase temperature
T_{init}	Ignition temperature
$T_{initial}$	Initial temperature of the sample
$T_{initial}=-1/\gamma$	

The first page (with annotation) only for English language papers

c_{Pk}	Specific capacity at constant pressure $(\mathrm{J/kg/K})$
$\rho_{1g}=\rho_{N2},\ \rho_{1s}=\rho_{Zr},\rho_{2s}=\rho_{ZrN}$	Densities of gas and solid species $(kg\cdot m^{-3})$
$\rho_g=\rho_{1g}+\rho_{2g}+\rho_{3g}$	Density of gas mixture $(kg\cdot m^{-3})$
$v_{jS}=\frac{M_{jS}}{\rho_{jS}}$	Molar volume of solid component
$\omega=\sum_{k=1}^{3}\varepsilon_{kk}$	First invariant of deformation tensor
σ_{ij}	Stress tensor for solid phase (Pa)
$\sum_k \sigma_{kk}=(2\mu_{S1}+3\mu_{S2})\sum_k \varepsilon_{kk}-3K\omega$	Thermo-elasticity relation (Pa)
$\sigma_{ij}=2\mu_{S1}\varepsilon_{ij}+\delta_{ij}\left(\mu_{S2}\sum_k \varepsilon_{kk}-K\omega\right)$	Duamel-Neuman formulas
$\omega=\omega_T+\omega_g+\omega_S$	Total expansion (dimensionless)
μ_{S1},μ_{S2}	Lame coefficients (Pa)
ω_g,ω_S	Concentration expansions
ω_T	Thermal expansion (dimensionless)
E_1	Activation energy $(\mathrm{J\cdot mole^{-1}})$
K	Volumetric expansion coefficient (Pa)
$\bar{\alpha}_{ig}$, $\bar{\alpha}_{iS}$	Species expansion coefficients (dimensionless)
$\beta_k=\frac{RT_0}{E_k},k=1,2$	Dimensionless parameters
$\gamma=\frac{c_P T_0 \beta_1}{Q}$	
ε_{ij}	Tensor of deformations (dimensionless)
$Pe_l=\frac{u_0 l_0}{D_{l,0}},l=1,2,\ Pe_T=\frac{u_0 l_0}{\lambda_0}$	Peclet numbers (dimensionless)

The first page (with annotation) only for English language papers

$u_0 = \frac{l_0}{t_0}$	Referred velocity $(m \cdot s^{-1})$
$\mathrm{Re}_0 = \frac{u_0 l_0 \rho_0}{\mu_0}$	Reynolds number (dimensionless)
R_{Solid}	The Reynolds number analog for solid phase
χ	Porosity coefficient (dimensionless)
κ	Thermal transfer coefficient $WK^{-1}m^{-2}$;
P_0 ,	Referred pressure (Pa)
μ_0	Referred gas viscosity $(kg \cdot m^{-1} \cdot s^{-1})$
λ_0	Referred thermal conductivity $(W \cdot m^{-1} \cdot K^{-1})$
Ma_0	Mach number (dimensionless)
$M_{1g}, M_{2g}, M_{jS},\ j = 1,2$	Molar masses $(kg \cdot mole^{-1})$
$\mathrm{Q_f}$	Thermal flux $(W \cdot m^{-2})$
$\mathrm{Q}_r, k, \tilde{Q}_r = \frac{Q t_0 k}{\rho_0 C_{pg} T_0},\ \tilde{k} = t_0 k$	Combustion heat and fate $(W \cdot m^{-2})$, (s^{-1})
Q_{Tg}, Q_{Ts}	Heat fluxes due to chemical reaction $(W \cdot m^{-2})$
Q	Creep activation energy in the power law $(J \cdot mole^{-1})$
$Pe_T = \frac{l_0^2 \rho_0 c_p}{t_0 \lambda_0}$	Peclet number for gas phase (dimensionless)
$Pe_{Ts} = \frac{l_0^2 \rho_0 c_{ps}}{t_0 \lambda_s}, Pe_{gr} = \frac{l_0^2 \rho_{gr} c_{p,\mathrm{gr}}}{t_0 \lambda_{gr}}$	Peclet numbers for solid phases (dimensionless)
$Pe_{el} = \frac{l_0^2 \rho_{el} c_{p,el}}{t_0 \lambda_{el}},$	Peclet number for wolfram tungsten (dimensionless)
Q_{Joul}	Joul ‘s heat due to electric current in a tungsten channel $(W \cdot m^{-2})$
$\tilde{j} = \sigma_{el} E_{el,0}$	Electric current (A)
	Electric current (A), electric potential (V)

$j = \sigma E$, $\varphi_0 = l_0 E_{el,0}$

$q_{g,rad}$	The thermal radiation / absorption heat flux $(W \cdot m^{-2})$
$A_W = \frac{2\chi l_0^2}{r_p}\frac{\sigma_B}{\lambda_0}T_0^3$, ε_Σ , $\frac{1}{\varepsilon_\Sigma} = \frac{1}{\varepsilon_g} + \frac{1}{\varepsilon_s}$	Boltzmann's constant, emissivity
D_T	Thermal diffusivity coefficient $(\mathrm{W \cdot m^{-1} \cdot K^{-1}})$
$R = 8.314$	Gas constant $(\mathrm{J \cdot mole^{-1} K^{-1}})$
t_{init}	Ignition time
$q_f(t)$	External heat flux $(W \cdot m^{-2})$
N_{2f}	External nitrogen flux $(\mathrm{kg} \cdot m^{-2} \cdot s^{-1})$
$\dot{\gamma}$, $\dot{\gamma} = \dot{\gamma}_0 \exp\left(\frac{-Q}{RT}\right)$	Plastic deformation, densification rate
ΔG	Activation energy of plastic deformation, (kJ / mol)
$\varphi = (1-\chi)^2$	Normalized shear modulus (dimensionless)
$\psi = \frac{2}{3}\frac{(1-\chi)^3}{\chi}$	Normalized bulk modulus (dimensionless)
$\sigma(W)$	Equivalent stress for the power law, $\sigma(W) = A_m \cdot W^m$
$\sigma_{z,ole}$, $\dot{\chi}_{ole}$	Stress, densufucation rateusing model [41]
P_L	Effective stress of free sintering (dimensionless)
P_{ex}, P_g	External pressure, gas pressure at the pore boundary
$P_{tot} = P_{ex} - P_g$	Total pressure (Pa)
$\dot{\varepsilon}_{ij}$	Strain rate tensor (dimensionless)
A , A_0	Creep coefficients for the power law, $A_m = \frac{A_0 T}{r_p}\left(\frac{d}{b}\right)^p \exp\left(\frac{-Q}{RT}\right)$ (dimensionless)
$\backslash i_{elast}(t,x,r) = \begin{cases} 1, & \chi < \zeta\chi_0 \\ 0, & \chi \geq \zeta\chi \end{cases}$	Thermal elasticity/plasticity criteria (dimensionless)

The first page (with annotation) only for English language papers

$\zeta = \dfrac{(1-10^{-3})G_1}{G_0}$

$G_1 = \dfrac{\rho_{2s}}{M_{2s}} - \dfrac{\rho_{1s}}{M_{1s}} - \dfrac{\rho_{1g}}{M_{1g}}, G_0 = \dfrac{\rho_{2s}^0}{M_{2s}} - \dfrac{\rho_{1s}^0}{M_{1s}} - \dfrac{\rho_{1g}^0}{M_{1g}}$

$\dfrac{r_P - r_P^0}{r_P^0} = 0.2\%$

Thermal elasticity/plasticity criteria for solid particle

$n_P = N_A \cdot V_P / V_0$

$n_P\ (mol^{-1}),\ N_A = 6 \cdot 10^{23}\ (mol^{-1})$

r_P , V_P

Radius, volume of solid particle, $r_P \approx 5 \cdot 10^{-7}\ (m)$

Subscripts: g, s, zero

Gas, solid, initial value